Mechanics of Advanced Composite Structures 10 (2023) 167 – 194

Semnan University

Mechanics of Advanced Composite Structures

journal homepage: http://MACS.journals.semnan.ac.ir

Free Vibration Response of Agglomerated Carbon Nanotube-Reinforced Nanocomposite Plates

M. C. Maurya [a*], S. M. A. Jawaid [a], A. Chakrabarti [b]

[a] *Department of Civil Engineering, Madan Mohan Malaviya University of Technology, Gorakhpur-273010, India*
[b] *Department of Civil Engineering, Indian Institute of Technology, Roorkee-247667, India*

KEYWORDS

FE method;
HSDT;
Eshelby-Mori-Tanaka;
Carbon nanotubes;
Frequency.

ABSTRACT

The current investigation deals with the effect of carbon nanotube (CNT) agglomeration on the free vibration behavior of nanocomposite plates created by inserting various graded distributions of carbon nanotube (CNT) in a polymeric matrix. In this study, affected material properties because of the CNT agglomeration effect were estimated first according to the two-parameter agglomeration model based on the Eshelby-Mori-Tanaka approach for randomly oriented carbon nanotubes, and then a FEM code has been developed to model the FG plate using third-order shear deformation theory. In the used higher-order shear deformation theory, transverse shear stresses are represented by quadratic variation along the thickness direction, resulting in no need for a shear correction factor. Next, the present approach is implemented with the FEM by employing a C^0 continuous isoparametric Lagrangian FE model with seven nodal unknowns per node. Finally, the effect of various levels of agglomeration by altering the agglomeration parameters, different CNT distribution patterns across the thickness direction, and various side-to-thickness ratios along with various boundary conditions on the free vibration response of CNT reinforced composite plates explored parametrically. The generated result shows that the CNT agglomeration effect has a significant impact on the natural frequencies of the nanocomposite plate.

1. Introduction

The work of Iijima [1,2] enabled scientists to comprehend the enormous potential of Carbon Nanotubes (CNTs) and piqued the curiosity of many researchers who set out to find a practical use for CNTs that would benefit from them. Because of their superior mechanical and thermal qualities, carbon nanotubes (CNTs) have been recognized as the ideal candidate for reinforcing composite materials that may be used in a wide range of technological disciplines, including aerospace and mechanical engineering, since their discovery [3]. Functionally graded carbon nanotube-reinforced composites (FG-CNTRCs) have received a lot of interest in recent years due to their exceptional mechanical properties. FG-CNTRC structures have numerous potential applications in aerospace, civil and ocean engineering, the automotive industry, and smart structures [41]. Nonetheless, as seen by many publications published on the subject, the characterization of the mechanical properties of CNTs is still an unresolved question [4]. Several ways to define the mechanical behavior of such composites can be discovered in the literature. They are commonly used for various structural purposes to improve the dynamic response or to provide a superior attitude in particular buckling issues. As a result of these considerations, it was decided to investigate the effect of CNT insertion into the polymeric matrix with various distributions and the agglomeration effect.

The simplified method for determining Young's moduli, shear moduli, and Poisson's ratios of a CNT-reinforced layer with orthotropic properties is to use an extended version of the Rule of Mixture, which can be found in [5]. The studies of Alibeigloo and Liew [6] and Alibeigloo [7], in which the elasticity is applied to explore the thermal and dynamic behavior of various

* Corresponding author. Tel.: +91-9451800047
E-mail address: mcmce@mmmut.ac.in

DOI: 10.22075/macs.2022.28148.1430
Received 2022-08-21; Received in revised form 2022-11-07; Accepted 2022-11-12.

CNT-reinforced composite structures, respectively, provide some examples of this approach in use. The books of Alibeigloo and Liew [6] and Alibeigloo [7] contain examples of these uses.

In their most recent publications [8,9], Zhang, Lei, and Liew characterize the engineering constants of the material using the same micromechanical method to assess the mechanical properties of these composites. In these studies, the free vibration analysis is numerically solved using an upgraded version of the conventional Ritz approach.

Shi et. al. [10] suggest a strategy that is entirely distinct from any other one that has been used before to explore the CNTs agglomeration effect using a two-parameter theoretical model. The foundation of this concept is based on the idea that the spatial distribution of CNTs inside the matrix is not uniform, and as a consequence, certain regions of the composite material have a larger reinforcing particle concentration than others. After that, an evaluation of the effective mechanical characteristics of the composite, which in this instance possesses isotropic overall features, is carried out using a homogenization method that is based on the popular Mori-Tanaka method for granular composite materials [11]. The works [4,12], which present some parametric investigations to look into the impact that CNT agglomeration has on the vibrational behavior of various basic structures, take into account the current strategy. The purpose of these studies is to determine whether or not CNT agglomeration is beneficial.

Hedayati and Sobhani Aragh have especially considered the impact of graded agglomerated CNTs on annular sectorial plates' free vibration behavior sitting on the Pasternak foundation [12]. On the other hand, Sobhani Aragh et al. have evaluated the natural frequencies of CNT-reinforced cylindrical shells [4,13]. In the research that was carried out and presented by Giovanni et. al. [14], the composite plates were assumed to be made of a purely isotropic elastic hosting matrix of one of three distinct types (epoxy, rubber, or concrete) and embedded single-walled carbon nanotubes. The computations are done by discretizing the composite plates as finite elements using the finite element method (FE). It is determined how the modal characteristics are changed both locally and globally by the impacts of the CNT alignment and volume percentage, and it is then demonstrated that the lowest natural frequencies of CNT-reinforced rubber composites can rise by up to 500 %. To generate and precisely solve the equations of motion, the analysis technique is based on the FSDT [15]. This is accomplished in order to record the fundamental frequencies of the rectangular functionally graded (FG) plates that are supported by an elastic base. Through the use of the finite element method, the purpose of this study is to ascertain the natural frequencies of an isotropic thin plate. The frequencies that were calculated have been contrasted with those that were determined using an exact Levy-type solution. The Kirchhoff plate theory is used as the foundation for the calculation of the stiffness and mass matrices, which are done using the finite element method (FEM). The natural frequencies of the considered rectangular plate can be obtained with the help of this methodology, which is useful [16]. The impact of CNT agglomeration on the elastic characteristics of nanocomposites is assessed using a two-parameter micromechanics model of agglomeration. In this research, an analogous continuum model based on the Eshelby-Mori-Tanaka method is used to determine the effective constitutive law of an elastic isotropic medium (matrix) with oriented straight CNTs. The results of this research work are presented in this article. The discretization of the equations of motion and the implementation of the various boundary conditions are both accomplished through the use of the generalized differential quadrature method (GDQM) for two dimensions [12]. With four unknowns, a new higher-order shear deformation theory has been devised, but it takes into consideration the transverse shear strains' parabolic fluctuation across the plate thickness. The flexure and free vibration analysis of FG plates is done using this theory. Therefore, a shear correction factor is not required to be used. The findings indicate that the present theory is capable of achieving the same level of precision as the existing higher-order theories of shear deformation, despite the latter's greater number of unanswered questions; however, the present theory's precision cannot be compared to that of 3D and quasi-3D models that take into account the effect of thickness stretching [17]. Zhang et. al. [9] used both the element-free IMLS-Ritz technique and first-order shear deformation theory, also known as FSDT, to account for the impact of the plate's transverse shear deformation. The study investigated how the vibration behavior of the plate was affected by various factors, including the volume fraction of carbon nanotubes, the plate's thickness-to-width ratio, the plate's aspect ratio, and the boundary condition. Mareishi et. al. [5] studied the nonlinear free and forced vibration behavior of advanced nano-composite beams resting on nonlinear elastic foundations. SWCNT volume fractions and dispersion patterns affect system behavior. Researchers studied the nonlinear forced and free vibration response of smart laminated nano-composite beams and

discovered this. Tornabene et. al. [18] looked at how agglomerated CNT affected the free vibration behavior of laminated composite plates and double-curved shells. They used Carrera Unified Formulation (CUF), which is a method that permits the consideration of multiple Higher-order Shear Deformations Theories (HSDTs). Kiani [19] looked at how CNT-based nano-composite plates that had layers of piezoelectric material on the top and bottom behaved when they were free to move. During the course of the research, the properties of the composite medium were determined with reference to a revised version of the rule of mixtures method that incorporates efficiency parameters. The electric potential was thought to be spread out in a straight line across the thickness of the piezoelectric material. The full set of motion and Maxwell equations for the system were found by using the Ritz formulation, which works for any in-plane and out-of-plane boundary conditions. These equations describe the system's behavior. In this case, the researcher takes into consideration both open circuits and closed circuits as potential electrical boundary conditions for the free surfaces of the piezoelectric layers. According to the findings of the study, the resultant eigenvalue system was successfully solved in order to get the system's frequencies as well as the mode shapes. In the end, it was determined that the fundamental frequency of a plate with a closed circuit always had a higher value than the fundamental frequency of a plate with open circuit boundary conditions. A new eight-unknown shear deformation theory was developed by Nguyen et. al. [20] for the bending and free vibration study of FG plates using the finite-element method. The presented theory concurrently fulfills zeros for the transverse strains at the top and bottom surfaces of FG plates and is based on a full 12-unknown higher-order shear deformation theory. The research utilized a rectangular element with four nodes and sixteen degrees of freedom at each node. In the end, the results were checked against the results that were already published in the relevant literature. Over the course of the research, parametric studies were carried out for a variety of power-law indices and side-to-thickness ratios. Using both experimental measurements and an analytical method, Moghadam et. al. [21] investigated the effect of CNT agglomerates on the residual stresses in a fiber-reinforced nanocomposite. In order to calculate the residual stress that was caused by thermal treatment, an analytical solution was utilized, which was founded on the traditional laminate theory. The observed residual stresses acquired using the incremental hole-drilling method were found to be in good agreement with the theoretical residual stresses computed by each layer of the laminates. The study's findings demonstrated that poorly dispersed samples produced higher residual stresses when compared to perfectly dispersed samples, and this phenomenon was found to be more significant in the case of nanocomposites containing higher weight fractions of CNTs. Hamid et al. [22] studied the free vibration of size-dependent CNTRC nanoplates on a visco-Pasternak foundation. Maleki et al. [23] solved the free vibration problem of three-phase carbon fiber/nanotube/polymer nanocomposite conical shells using the GDQM. This was done in order to address the impact that the agglomeration of carbon nanotubes (CNTs) has on the dynamic responses of the shell. The final finding of the study was that the presence of agglomeration phenomena can significantly alter the dynamic behavior of the nanocomposite structure. Zhang et al. [34,35] studied the vibration analysis of carbon nanotube (CNT) reinforced functionally graded composite triangular plates subjected to in-plane stresses and also investigated the effect of in-plane forces on the vibration behavior of carbon nanotube (CNT) reinforced composite skew plates using first-order shear deformation theory. Zhang and Salem [36] investigated the free vibration behavior of carbon nanotube (CNT) reinforced functionally graded thick laminated composite plates utilizing Reddy's higher-order shear deformation theory (HSDT) in combination with element-free IMLS-Ritz method with four types of CNT distributions. Finally, the influence of boundary conditions on the sequence of the first six mode shapes for various lamination arrangements is studied in detail. Mehar and Panda [37] studied in detail the vibration characteristics of carbon-nanotube-reinforced sandwich curved shell panels under the elevated thermal environment using the higher-order shear deformation theory. Mehar et. al. [38-40] have done extensive theoretical and experimental investigations of vibration characteristics of carbon-nanotube reinforced polymer composite structures.

In conclusion, from the above-detailed literature review, the current manuscript is structured in a manner that helps to incorporate the CNTs agglomeration effect as can be seen that CNTs tend to agglomerate for low-volume fraction distribution. Hence, if the above-mentioned effect is not considered, will lead to erroneous results for the structures built from these CNT materials. The current work focuses on the analysis of functionally graded CNT reinforced plates, including the effect of agglomeration with different CNT distribution patterns, aspect ratio, and boundary conditions regarding its influence on the natural frequency

of plate structure only. The analysis is based on the finite element method using Reddy's HSDT model. The material properties of agglomerated CNTs are evaluated based on the Eshelby-Mori-Tanaka method.

2. Material Modelling

For any structural analysis, material modeling is very important. The application of CNT-reinforced composite structures, demands to development of detailed modeling of the effective material properties of a such composite at the macroscopic level. Because molecular dynamics or other atomistic models are computationally intensive, micromechanical methods are used to describe the behavior of these materials in this work.

Material modeling of FG-CNTRC is presented using the Mori-Tanaka method, considering the effect of agglomeration of CNT for various types of CNT distributions.

2.1. Material Modeling of FG-CNTRC

The FG-CNTRC material is considered to be made up of an isotropic matrix (e.g., epoxy resin) and fiber (CNTs), with material qualities graded along the direction of thickness of the plate as per linear distribution (UD and FG-V) of the fraction of volume of CNTs (fig.1).

The volume fractions (V_{cnt}) of CNTs in four types of functionally graded carbon nanotube plates are stated as follows:

$$\begin{aligned} V_{cnt} &= V_{cnt}^{*} \qquad (UD) \\ V_{cnt} &= \left(1+\frac{2z}{h}\right)V_{cnt}^{*} \quad (FG-V) \\ V_{cnt} &= 2\left(1-\frac{2|z|}{h}\right)V_{cnt}^{*}(FG-O) \\ V_{cnt} &= 2\left(\frac{2|z|}{h}\right)V_{cnt}^{*} \qquad (FG-X) \end{aligned} \tag{1}$$

$$V_{cnt}^{*} = \frac{w_{cnt}}{w_{cnt}+\frac{\rho_{cnt}}{\rho_m}-\left(\frac{\rho_{cnt}}{\rho_m}\right)w_{cnt}} \tag{2}$$

where, w_{cnt} represents the CNTs mass fraction and ρ_{cnt} and ρ_m the densities of carbon nanotube and matrix, respectively. The material properties can be determined for this linear material property fluctuation by putting the value of V_{cnt}^{*} into Eq. (1) for linear material property variation.

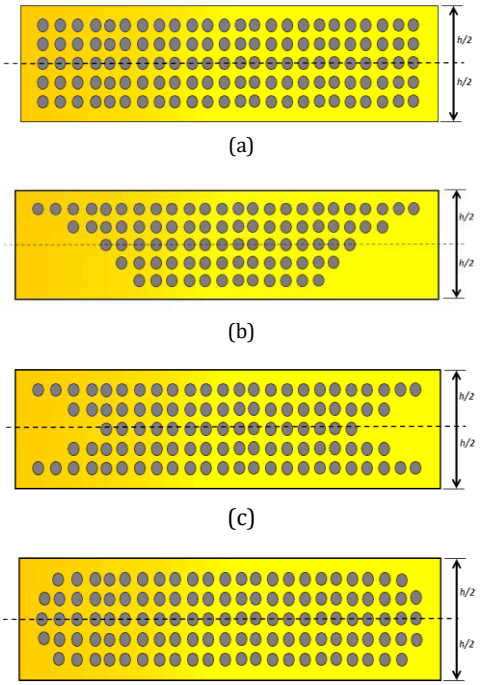

Fig. 1. (a) Uniformly distributed CNT nanocomposite plate, (b) V-Shape distributed CNT nanocomposite plate, (c) X-Shape distributed CNT nanocomposite plate, (d) O-Shape distributed CNT nanocomposite plate.

2.2. Modeling of Nanocomposite Material:

Several micromechanical models have been proposed to predict the properties of the material of CNT-reinforced composites. In this research, the Mori–Tanaka technique is used to estimate the elastic properties of the equivalent fiber/polymer material. The equivalent inclusion average stress technique, commonly known as the Eshelby–Mori–Tanaka method, is based on Eshelby's [8] equivalent elastic inclusion notion and Mori-Tanaka's [6] concept of average stress inside the matrix. Benveniste's [9] revision of the effective modulus of elasticity tensor C of CNT-reinforced composites is as follows:

$$C = V_{cnt}\left\langle (C_r - C_m)A\right\rangle\left(V_m I + V_{cnt}\left\langle A_r\right\rangle\right)^{-1} + C_m \tag{3}$$

The symbol *I* is denoted as a fourth-order unit tensor. The matrix stiffness tensors are C_m, while the equivalent fiber stiffness tensors are C_r (CNT). The angle brackets in their overall configuration represent an average of all possible orientations for the inclusions. A_r is the tensor of the concentration of dilute mechanical strain, and it can be calculated as follows:

$$A_r = \left[I + S\left(C_r - C_m\right)(C_m)^{-1}\right]^{-1} \tag{4}$$

here symbol S represents the Eshelby tensor of the fourth order, as defined by Mura and Eshelby [8,10].

Here, a single-walled carbon nanotube having a solid cylinder of 1.424 nm diameter with (10,10) chirality index [11] is used for the analysis.

2.2.1. Randomly Oriented CNT-Reinforced Composites:

Two Euler angles show straight carbon nanotube orientation α and β, denoted by the arrows in Fig. 2. As a result, the base vectors $\vec{e}_i$ of the global $(0{-}x_1\,x_2\,x_3)$ coordinate system and the base vectors $\vec{e}_i'$ of $(0{-}x_1'\,x_2'\,x_3')$ the local coordinate system are produced, which are related through the transformation matrix g, as follows:

$$\vec{e}_i = g\vec{e}_i^{\,r} \tag{5}$$

where g is given as:

$$g = \begin{bmatrix} \cos\beta & -\sin\beta\cos\alpha & \sin\beta\sin\alpha \\ \sin\beta & \cos\beta\cos\beta & -\cos\beta\sin\alpha \\ 0 & \sin\alpha & \cos\alpha \end{bmatrix} \tag{6}$$

It is possible to characterize the orientation distribution of carbon nanotubes in composites by a function of probability density $p(\alpha, \beta)$ that meets the normalizing condition.

$$\int_0^{2\pi}\int_0^{\pi/2} p(\alpha,\beta)\sin\alpha\, d\alpha\, d\beta = 1 \tag{7}$$

Considering the random CNT orientation, the function of density for this case is,

$$p(\alpha,\beta) = \frac{1}{2\pi} \tag{8}$$

Calculation of Hill's elastic moduli for the reinforcing phase was accomplished by analyzing the equivalence of the two matrices that are presented below [13]:

$$C_r = \begin{bmatrix} n_r & l_r & l_r & 0 & 0 & 0 \\ l_r & k_r+m_r & k_r-m_r & 0 & 0 & 0 \\ l_r & k_r-m_r & k_r+m_r & 0 & 0 & 0 \\ 0 & 0 & 0 & p_r & 0 & 0 \\ 0 & 0 & 0 & 0 & m_r & 0 \\ 0 & 0 & 0 & 0 & 0 & p_r \end{bmatrix}$$

$$= \begin{bmatrix} \frac{1}{E_L} & \frac{-\nu_{TL}}{E_T} & \frac{-\nu_{ZL}}{E_Z} & 0 & 0 & 0 \\ \frac{-\nu_{LT}}{E_L} & \frac{1}{E_T} & \frac{-\nu_{ZT}}{E_Z} & 0 & 0 & 0 \\ \frac{-\nu_{LZ}}{E_L} & \frac{-\nu_{TZ}}{E_T} & \frac{1}{E_Z} & 0 & 0 & 0 \\ 0 & 0 & 0 & \frac{1}{G_{TZ}} & 0 & 0 \\ 0 & 0 & 0 & 0 & \frac{1}{G_{TZ}} & 0 \\ 0 & 0 & 0 & 0 & 0 & \frac{1}{G_{LT}} \end{bmatrix}^{-1} \tag{9}$$

the terms k_r, l_r, m_r, n_r, and p_r in Eq. (9) represent Hill's elastic moduli for the reinforcing phase (CNTs) of the composite calculated by the inverse of the compliance matrix of the equivalent fiber.

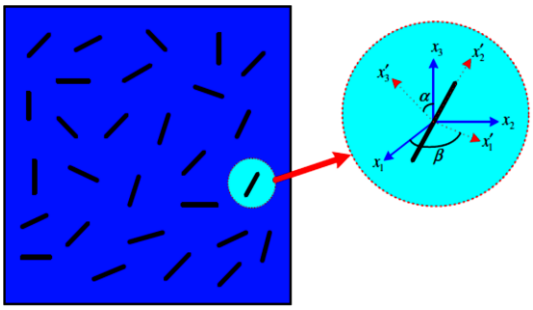

Fig. 2. Representative volume element (RVE) Composed of Randomly oriented straight CNT [12].

As for the composite's properties E_L, E_T, E_Z, G_{LT}, G_{TZ}, G_{TZ}, and ν_{LT}, which may be established using the rule of mixture technique, the first step is to determine the properties of the composite by performing a multiscale finite element analysis or molecular dynamics simulation analysis [14] on the composite.

Here, the composite is considered to be isotropic when the carbon nanotubes are orientated totally randomly in nature in the matrix. For this, the bulk modulus K and shear modulus G is calculated as follows:

$$K_{NC} = \frac{V_{cnt}\left(\delta_r - 3K_m\alpha_r\right)}{3\left(V_m + V_{cnt}\alpha_r\right)} + K_m \tag{10}$$

$$G_{NC} = \frac{V_{cnt}\left(\eta_r - 2G_m\beta_r\right)}{2\left(V_m + V_{cnt}\beta_r\right)} + G_m \tag{11}$$

The term K_m and G_m are used for bulk and shear moduli of the matrix, respectively.

$$\alpha_r = \frac{3\left(K_m + G_m\right) + k_r - I_r}{3\left(G_m + k_r\right)} \tag{12}$$

$$\beta_r = \frac{1}{5}\left[\frac{4G_m + 2k_r + I_r}{3\left(G_m + k_r\right)} + \frac{4G_m}{G_m + p_r} + \frac{2\left[G_m\left(3K_m + G_m\right) + G_m\left(3K_m + 7G_m\right)\right]}{G_m\left(3K_m + G_m\right) + m_r\left(3K_m + 7G_m\right)}\right] \tag{13}$$

$$\delta_r = \frac{1}{3}\left[n_r + 2I_r + \frac{\left(2k_r + n_r\right)\left(3k_m + 2G_m - I_r\right)}{G_m + k_r}\right] \tag{14}$$

$$\eta_r = \frac{1}{5}\left[\frac{2}{3}\left(n_r - I_r\right) + \frac{8G_m p_r}{G_m + p_r} + \frac{(3K_m + 4G_m)8m_r G_m}{G_m(7m_r + G_m) + 3K_m(m_r + G_m)} + \frac{2(I_r + 2G_m)(k_r - I_r)}{3(k_r + G_m)}\right] \tag{15}$$

Finally, the modulus of elasticity and Poison ratio of a CNT-based nanocomposite material are as follows:

$$E_{NC} = \frac{9KG}{G + 3K} \tag{16}$$

$$\nu = \frac{3K - 2G}{2(G + 3K)} \tag{17}$$

Additionally, V_{cnt} and V_m represent the volume fractions of the carbon nanotubes and matrix, respectively, which fulfill the expression $V_{cnt} + V_m = 1$. In a similar way, the mass density ρ is determined as follows:

$$\rho = \rho_{cnt} V_{cnt} + \rho_m V_m \tag{18}$$

where ρ_m and ρ_{cnt} represents the mass density of matrix and carbon nanotubes, respectively.

2.2.2. Agglomeration of Carbon Nanotubes

A large proportion of carbon nanotubes in carbon nanotube-reinforced composites has been found to be concentrated in agglomerates. Nanotubes agglomerate into bundles due to the van der Waals attractive interactions between them. After determining the material properties of FG-CNTRC without taking into account the CNT agglomeration effect, a new micromechanics model is developed and applied to a random oriented, agglomerated CNT-reinforced polymer composite to determine the effective properties of the material of a single-walled CNT reinforced polymer composite while taking into account the CNTs bundling effect. The influence of agglomeration on the elastic characteristics of CNT-reinforced composites having random orientation is investigated in the present study, which uses a two-parameter micromechanics agglomeration model to do this.

As per Fig. 3, it can be seen that the elastic characteristics of the surrounding material are distinct from the areas where inclusions have concentrated nanotubes.

2.2.2.1. Two Parameter Agglomeration Model

In polymer matrix, the major cause of agglomeration of carbon nanotubes is the small diameter, due to which the elastic modulus gets reduced and the aspect ratio increases in the radial direction and hence producing low bending strength. It is crucial that carbon nanotubes are dispersed uniformly inside the matrix to achieve the desired features of CNT-reinforced composites. Here, a micromechanical model has been built to check the CNTs agglomeration effect on the effectiveness of carbon nanotube-enhanced elastic modules.

Shi et al. [5] found that a substantial number of CNTs are concentrated in aggregates in the 7.5 % concentration sample. Carbon nanotubes are found to be unevenly distributed in the substrate, with a few areas having CNT concentrations larger than the average volume fraction. As illustrated in Fig. 3, these areas containing concentrated carbon nanotubes are considered spherical in this section and are referred to as 'inclusions' having a mix of varying elasticity characteristics from the surrounding material.

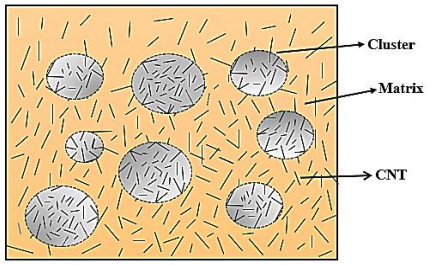

Fig. 3. Agglomeration of carbon nanotubes (CNTs) within the representative volume element (RVE)

The total volume V_r of CNTs in the RVE may be separated into two parts:

$$V_r = V_r^{inclusion} + V_r^m \tag{19}$$

where V_r^m and $V_r^{inclusion}$ are represented as the CNTs' volume dispersed in the matrix and the inclusions (concentrated regions), respectively.

To understand clearly the effect of carbon nanotube agglomeration, two parameters are introduced as ξ & ζ.

$$\xi = \frac{V^{inclusion}}{V}, \zeta = \frac{V_r^{inclusion}}{V_r} \tag{20}$$

where $V_r^{inclusion}$ represents the volume of the RVE's sphere inclusions. In this case, ξ represents the volume of the inclusion fraction in relation to the RVE's total volume V. Whenever ξ is equal to one, CNTs are assumed to be distributed uniformly in the matrix, and as the value of ξ decreases, the degree of agglomeration of carbon nanotubes becomes more severe (Fig. 5). The symbol ζ denotes the nanotubes volume ratio distributed in the inclusions to the total volume of the CNTs. When the value ζ is 1, all of the nanotubes are concentrated in the sphere regions. This is true if all nanotubes are dispersed evenly (i.e., $\zeta = \xi$) throughout the matrix. As the value of ζ increases (i.e., $\zeta > \xi$), the CNT's spatial distribution becomes more. V_{cnt} denotes the average carbon nanotube volume fraction in the composite as per Eq. (21).

$$V_{cnt} = \frac{V_r}{V} \tag{21}$$

The carbon nanotube volume fractions in the inclusions and the matrix are calculated using Eqs. (19)-(21), and they are expressed as

$$\frac{V_r^{inclision}}{V^{inclusion}} = V_{cnt} \frac{\zeta}{\xi} \tag{22}$$

$$\frac{V_r^m}{V - V^{inclusion}} = \frac{V_{cnt}(1-\zeta)}{1-\xi} \tag{23}$$

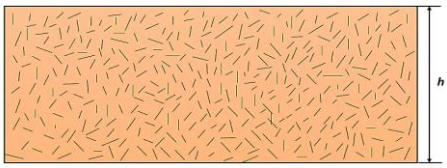

Fig. 4. $\varsigma = \xi = 1$ (Without agglomeration)

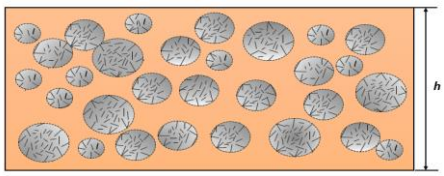

Fig. 5. $\varsigma = 1, \xi < \varsigma$ (Complete agglomeration)

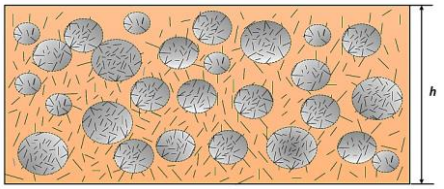

Fig. 6. $\varsigma < \xi, \xi < \varsigma$ (Partial agglomeration)

As a result, the Composite reinforced with carbon nanotubes is viewed as a system made up of sphere-shaped inclusions embedded in a hybrid matrix. CNTs can be found in both the matrix as well as in the inclusions also. Hence to compute the composite system's overall property, first, we have to estimate the inclusion's effective elastic stiffness and then the matrix.

Different micromechanics methods can be used to calculate the effective modulus of elasticity of the hybrid inclusions and matrix. Assuming that all CNT orientations are completely random and the nanotubes are transversely isotropic, the Mori-Tanaka scheme is used to estimate the hybrid matrix's elastic moduli, as described in the previous section. The carbon nanotubes are assumed to be oriented randomly within the inclusions, and thus the inclusions are isotropic. The term K_{in} and K_{out} represent the effective bulk moduli G_{in} and G_{out} represents the effective shear moduli of the inclusions and matrix, respectively given as:

$$K_{in} = K_m + \frac{V_{cnt}\zeta\left(\delta_r - 3K_m\alpha_r\right)}{3\left(\xi - V_{cnt}\zeta + V_{cnt}\zeta\alpha_r\right)} \tag{24}$$

$$K_{out} = K_m + \frac{V_{cnt}(1-\zeta)\left(\delta_r - 3K_m\alpha_r\right)}{\left[3\left(1-\xi - V_{cnt}(1-\zeta) + V_{cnt}(1-\zeta)\alpha_r\right)\right]} \tag{25}$$

$$G_{in} = G_m + \frac{V_{cnt}\zeta\left(\eta_r - 2G_m\beta_r\right)}{2\left(\xi - V_{cnt}\zeta + V_{cnt}\zeta\beta_r\right)} \tag{26}$$

$$G_{out} = G_m + \frac{V_{cnt}\left(\eta_r - 2G_m\beta_r\right)(1-\zeta)}{\left[2\left(1-\xi - V_{cnt}(1-\zeta) + V_{cnt}\beta_r(1-\zeta)\right)\right]} \tag{27}$$

Following that, the composite's effective bulk modulus K and effective shear modulus G are computed using the method of Mori-Tanaka as follows:

$$K = K_{out}\left[1 + \frac{\xi\left(\frac{K_{in}}{K_{out}} - 1\right)}{1 + \alpha(1-\xi)\left(\frac{K_{in}}{K_{out}} - 1\right)}\right] \tag{28}$$

$$G = G_{out}\left[1 + \frac{\xi\left(\frac{G_{in}}{G_{out}} - 1\right)}{1 + \beta(1-\xi)\left(\frac{G_{in}}{G_{out}} - 1\right)}\right] \tag{29}$$

where,

$$\nu_{out} = \left(\frac{3K_{out} - 2G_{out}}{2(3K_{out} + G_{out})}\right), \quad \alpha = \frac{(1+\nu_{out})}{3(1-\nu_{out})}, \beta = \frac{(8-10\nu_{out})}{(15-15\nu_{out})} \tag{30}$$

Finally, the CNT-reinforced composite's young modulus is calculated using Eq. (16).

3. Formulation

3.1. In-Plane Displacement Fields and Strains

The FGM plate's geometry used in this analysis is shown in Fig. 7. The plate's length and width are denoted by a and b, respectively, and its thickness is represented by h. The center of the FGCNT plate serves as the origin for material coordinates (x, y, and z). Plates are simply supported along their four edges, for the square plate. The aspect ratio considered is h/a = 0.1.

The in-plane displacement variation of *u*, *v*, and displacement in transverse direction *w* across the plate thickness may be described as using Reddy's theory of higher-order shear deformation [15].

$$\begin{aligned} u(x,y,z) &= u_0 + z\theta_x - \frac{4z^3}{3h^2}\gamma_x \\ v(x,y,z) &= v_0 + z\theta_y - \frac{4z^3}{3h^2}\gamma_y \\ w(x,y) &= w_0 \end{aligned} \tag{31}$$

where u_0, v_0 and w_0 signify the displacement of a point along the (x, y, z) coordinates located at mid-plane, respectively. θ_x and θ_y denotes the bending rotations in the y and x directions, respectively, and γ_x, γ_y denotes the shear rotations assumed in the x, and y directions.

The relationship between the strain component and the strain displacement is defined as follows:

$$\{\varepsilon_m\}=\begin{Bmatrix}\frac{\partial u}{\partial x}\\ \frac{\partial v}{\partial y}\\ \frac{\partial u}{\partial y}+\frac{\partial v}{\partial x}\\ \frac{\partial u}{\partial z}+\frac{\partial w}{\partial x}\\ \frac{\partial v}{\partial z}+\frac{\partial w}{\partial y}\end{Bmatrix}$$

$$=\begin{Bmatrix}\frac{\partial u_0}{\partial x}+z\frac{\partial \theta_x}{\partial x}-\frac{4z^3}{3h^2}\frac{\partial \gamma_x}{\partial x}\\ \frac{\partial v_0}{\partial y}+z\frac{\partial \theta_y}{\partial y}-\frac{4z^3}{3h^2}\frac{\partial \gamma_x}{\partial y}\\ \frac{\partial u_0}{\partial y}+z\frac{\partial \theta_x}{\partial x}-\frac{4z^3}{3h^2}\frac{\partial \gamma_x}{\partial x}+\frac{\partial v_0}{\partial y}+z\frac{\partial \theta_y}{\partial y}-\frac{4z^3}{3h^2}\frac{\partial \gamma_x}{\partial y}\\ \frac{\partial w_0}{\partial x}+\theta_x-\frac{4z^3}{h^2}\gamma_x\\ \frac{\partial w_0}{\partial y}+\theta_y-\frac{4z^2}{h^2}\gamma_y\end{Bmatrix} \quad (32)$$

The overall strain may be represented as mechanical strains for the purposes of plate analysis.

$$\{\varepsilon\}=\{\varepsilon_m\} \quad (33)$$

where ε_m represents the mechanical strain.

Again, in terms of total strain, the mechanical strain may be represented as

$$\{\varepsilon_m\}=[H]\{\varepsilon\} \quad (34)$$

while $[H]$ is the thickness coordinates-z function, and $\{\varepsilon\}$ is the function of x and y.

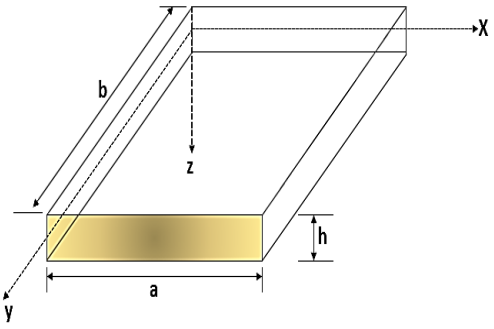

Fig. 7. Geometry of the FGCNT Plate

This describes the overall strain as,

$$\{\varepsilon\}=[H]\{\varepsilon\} \quad (35)$$

3.2. Constitutive Relationship

The relation between stress and strain for FGM is as follows:

$$\{\sigma\}=[Q]\{\varepsilon\} \quad (36)$$

where constitutive matrix

$$[Q]=\begin{bmatrix}Q_{11} & Q_{12} & 0 & 0 & 0\\ Q_{21} & Q_{22} & 0 & 0 & 0\\ 0 & 0 & Q_{33} & 0 & 0\\ 0 & 0 & 0 & Q_{44} & 0\\ 0 & 0 & 0 & 0 & Q_{55}\end{bmatrix} \quad (37)$$

In Eq. (37) the terms Q_{ij} are derived from the FG material properties, depending on the plate's thickness (z) as shown below in Eq. (38).

$$Q_{11}=Q_{22}=\frac{E}{1-\gamma^2}$$
$$Q_{12}=Q_{21}=\frac{\gamma E}{1-\gamma^2} \quad (38)$$
$$Q_{33}=Q_{44}=Q_{55}=\frac{E}{2(1+\gamma)}$$

3.3. Virtual work in FGCNT plate

The FGM plate's virtual work may be represented as

$$\delta U=\iiint\{\delta\varepsilon\}^T\{\sigma\}dx\,dy\,dz \quad (39)$$

With the help of Eq. (36), Eq. (39) can be rewritten as

$$\delta U=\iiint\{\delta\varepsilon\}^T[Q]\{\varepsilon\}dxdydz \quad (40)$$

The following equation can be extended further using Eq. (35) as follows:

$$\delta U=\iiint\{\delta\varepsilon\}^T[H]^T[Q][H]\{\varepsilon\}dxdydz \quad (41)$$

In Eq. (41) the matrix [Q] represents the constitutive matrix with elasticity derived from the constituent's elastic properties as given in Eq. (37). While *[H]* represents the 5 x 15 order matrix and includes the terms *z* and *h* as described below:

$$[H]=\begin{bmatrix}1&0&0&0&0&z&0&0&0&0&0&0&\frac{-4z^3}{3h^2}&0&0\\ 0&1&0&0&0&0&z&0&0&0&0&0&0&\frac{-4z^3}{3h^2}&0\\ 0&0&1&0&0&0&0&z&0&0&0&0&0&0&\frac{-4z^3}{3h^2}\\ 0&0&0&1&0&0&0&0&1&0&\frac{-4z^2}{h^2}&0&0&0&0\\ 0&0&0&0&1&0&0&0&0&1&0&\frac{-4z^2}{h^2}&0&0&0\end{bmatrix} \quad (42)$$

Finally, we can rewrite Eq. (41) as

$$\delta U=\iint\{\delta\varepsilon\}^T[D]\{\varepsilon\}dxdy \quad (43)$$

where matrix [D] represents the rigidity matrix vector. For which the corresponding expression is given in Eq. (44) shown below.

$$[D]=\int_{\frac{-h}{2}}^{\frac{h}{2}}[H]^T[Q][H]dz \quad (44)$$

4. Finite Element Formulation

4.1. Element Description

Figure 8 illustrates the isoparametric Lagrangian element's geometry with nine nodes used in the analysis. In this element, there is a total of sixty-three degrees of freedom because each node has seven degrees of freedom (*u, v, w*, θ_x, θ_y, γ_x and γ_y). In the x-y plane coordinate system, this element has a rectangular geometry that is completely arbitrary. The element is transferred to $\xi-\eta$ plane in order to get a rectangular geometry.

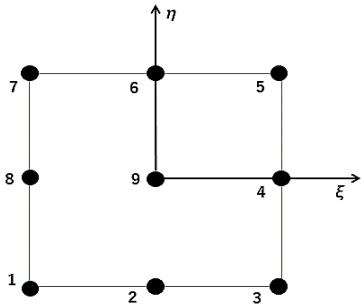

Fig. 8. Nine-noded Iso-parametric element with node numbering

For the present nine-node element the shape functions used are given below,

$$
\begin{aligned}
N_1 &= \frac{1}{4}(\eta-1)(\xi-1)\eta\xi,\\
N_2 &= \frac{1}{4}(\eta-1)(\xi+1)\eta\xi,\\
N_3 &= \frac{1}{4}(\eta+1)(\xi+1)\eta\xi\\
N_4 &= \frac{1}{4}(\eta+1)(\xi-1)\eta\xi,\\
N_5 &= -\frac{1}{2}(1-\eta)(1-\xi^2)\eta,\\
N_6 &= \frac{1}{2}(\eta^2-1)(1+\xi)\xi\\
N_7 &= -\frac{1}{2}(\eta+1)(\xi^2-1)\eta,\\
N_8 &= -\frac{1}{2}(\eta^2-1)(\xi-1)\xi,\\
N_9 &= (1-\xi^2)(1-\eta^2)
\end{aligned}
\tag{45}
$$

The relationship between strain and displacement can be established using the nine shape functions mentioned above. The vector of a strain can be expressed in the following way:

$$\{\varepsilon\} = [B]\{X\} \tag{46}$$

In Eq. (46) matrix [B] represents the strain-displacement matrix and matrix [X] represents the vector of nodal displacement for the element chosen and both matrices can be represented as follows:

$$
\begin{aligned}
[B] &= [B_1 \;\; B_2 \;\; B_3 \;\; B_4 \;\; B_5 \;\; B_6 \;\; B_7 \;\; B_8 \;\; B_9],\\
\{X\} &= [X_1 \;\; X_2 \;\; X_3 \;\; X_4 \;\; X_5 \;\; X_6 \;\; X_7 \;\; X_8 \;\; X_9]
\end{aligned}
\tag{47}
$$

4.2. Governing Equation for The Analysis of Free Vibrations

Mid-surface displacement parameters (u_o, v_o and w_o) can be used to calculate acceleration at any location within the element, as

$$\{\ddot{f}\} = \frac{\partial^2}{\partial t^2}\{\bar{f}\} = -\omega^2[F]\{f\} \tag{48}$$

In the above Eq. (48) the vector $\{f\}$ represents the nodal unknowns which is of order 7 x 1 and contains the terms of Eq. (33).

Again, the matrix $\{f\}$ is decoupled into matrix [C] which contains the shape functions (N_i) and global displacement vector $\{\delta\}$.

$$\{f\} = [C]\{\delta\} \tag{49}$$

The mass matrix of an element can be expressed using Eq. (48) and (49),

$$[m] = \iint_A [C]^T [L][C]\,dA \tag{50}$$

where the matrix [L] expression can be represented as

$$[L] = \int_z \rho[F]^T[F]\,dz \tag{51}$$

while ρ is the estimated density of the composite material from Eq. (18). As a result, the governing equation for free vibration analysis is,

$$([K]-\omega^2[M])\{X\} = \{0\} \tag{52}$$

5. Numerical Results & Discussion

In this section, many numerical examples were studied for the free vibration behavior of functionally graded nanocomposite plates with different distributions of carbon nanotube (Fig. 1) has been done by considering various agglomeration stages as shown in Figs. 4-6. This section is separated into two distinct sections. The first phase involves a convergence study and validation of the current formulation for isotropic plates [16] with varying aspect ratios, as no solution exists for the current problem. After confirming the effectiveness of the current formulation, the second step investigates the impacts of various agglomeration stages on the nondimensional frequency of the plate. In all the above phases, the influence of different boundary conditions (SSSS, CCCC, SCSC & SFSF) with different CNT distributions are investigated considering three stages of agglomeration (Fig.4) as (without agglomeration case), (complete agglomeration case) and (partial agglomeration

case) are investigated. The properties of SWCNT (10,10) are listed in Table 1. The matrix substance employed in this situation has the following elastic characteristics: E_m = 2.1 GPa, υ_m = 0.34, ρ_m = 1150 kg/m^3, and Table 1 lists the material characteristics of the reinforcement. The UD, FG-V, FG-X, and FG-O type reinforcement distributions with various levels of agglomeration testing were taken into consideration. 7.5% of the value is taken into consideration, which is a significant number of carbon nanotubes [30].

Here, before the verification and convergence study the mechanical properties were verified with the experimental work done by Odegard et al. [33] and presented in Fig. 9. From Fig. 9 it can be observed that the Eshelby-Mori-Tanaka scheme proposed by Shi et. al. [10] for the estimation of material properties and the results generated by Odegard et al. [33] are very close for the prediction of mechanical properties.

The result produced by the EMT approach for the agglomeration parameter ξ= 0.4 corresponding to ζ=1 (resembles the complete agglomeration behavior) is plotted in Fig. 9 with good agreement. The material for the matrix is used as E_m = 0.85 GPa and υ_m = 0.3, combined with the CNT properties given in Table 1 using the EMT approach to calculate overall mechanical properties for the analysis. The results generated here show, at the value of parameter ξ= 1 Young's modulus has the higher increase in function of volume fraction, and as the value of ξ decreases, the increase in the CNT volume fraction does not correspond to the expected increase of mechanical properties because of the severity of the agglomeration effect.

Fig. 9 itself is self-explanatory, and at the highest values of Young's modulus, both agglomeration parameters are considered equal values. It is also possible to observe that the variation of the parameter of ξ has a higher impact on mechanical properties as compared to other parameters ζ. After a thorough study of the effect of two agglomeration parameters (ζ,ξ) on overall elastic properties, three different stages of agglomeration are generated in the next section to understand the free vibration behavior of square plate with four types of CNT distribution patterns along the thickness direction as shown in Figs. 4-6.

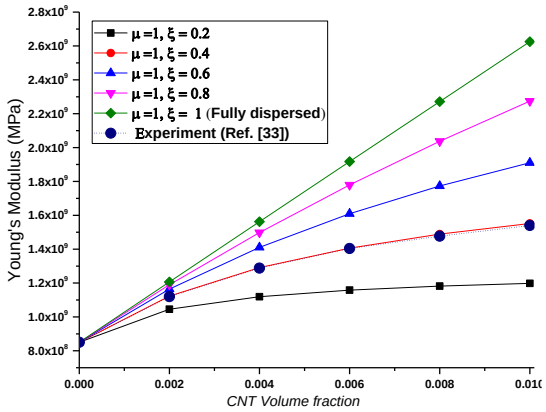

Fig. 9. Young's modulus for different levels of agglomeration and CNT volume fraction

Table 1. Hill's elastic moduli for Single-Walled Carbon Nanotubes (SWCNT) [31].

Carbon nanotubes	k_r[GPa]	l_r[GPa]	m_r[GPa]	n_r[GPa]	p_r[GPa]
SWCNT (10,10)	271	88	17	1089	442

Table 2. First six natural frequencies in Hz for isotropic plate (L = 0.6 m, B = 0.4 m) [16].

	Plate thickness h = 0.00625		Plate thickness h = 0.0125		Plate thickness h = 0.025		Plate thickness h = 0.05	
Mode No.	Ref.[16]	Present	Ref.[16]	Present	Ref.[16]	Present	Ref.[16]	Present
1	136.5	136.60	273.1	272.48	546.2	540.74	1092.5	1050.91
2	262.6	263.35	525.2	523.17	1050.4	1030.71	2100.9	1957.18
3	420.1	419.76	840.3	834.01	1680.7	1630.81	3361.5	3359.37
4	472.7	474.51	945.4	938.67	1890.8	1828.95	3781.7	3822.49
5	546.2	547.49	1092.5	1082.78	2185.0	2102.56	4370.1	4443.28
6	756.35	761.65	1512.7	1495.83	3025.4	3031.09	6050.8	6072.08

5.1. Validation Study-Isotropic Plate Under Free Vibration Case

A convergence study was carried out for free vibration analyses of agglomerated CNT-reinforced functionally graded plates in order to determine the appropriate number of mesh sizes that should be used in order to achieve accurate results.

The convergence analysis for a simply supported FG-CNT-reinforced plate at the fundamental frequency is shown in Table 2. The results are computed for V_{cnt}^{*} = 0.075 and a/h = 10 for different mesh sizes. Based on the results of these convergence studies, it has been determined that a mesh size of 16 x 16 is suitable for free vibration analysis of FG-CNT-reinforced plates. The outcomes of the free vibration analyses for an isotropic square plate are presented in Table 1 (E = 70 GPa, ρ = 2700 kg/m^3, and υ = 0.3). A comparison was made between the dimensionless frequency parameter of the isotropic plate and the HSDT results for a moderately thick plate [37].

5.2. Validation Study- FGM Plate Under Free Vibration Effect

A simply supported FGM plate consisting of aluminum (ceramic) and zirconium oxide (metal) is considered in the present problem. The properties of the constituents are: E_c = 151 GPa; E_m = 70 GPa; $\Upsilon_c = \Upsilon_m = 0.3$; ρ_c = 3000 kg/m^3; ρ_m = 2707 kg/m^3.The non-dimensional natural frequency parameter used in the present study is $\varpi = \omega\sqrt{12(1-\upsilon^2)\rho_c a^2 b^2/\pi^2 E_c h^2}$.

In Table 3, the natural frequency obtained from the present study is compared with the results of Talha et. al. [32], which are also based on higher-order shear deformation theory. The thickness ratio (a/h) is taken as 20 and the volume fraction index (n) is varied from 0.5 to 10.

Table 3. Variation of the frequency parameter with the volume fraction index, n, for SSSS square (Al/ZrO2) FGM plates (a/h = 20)

Mode	n = 1		n = 5	
	Ref. [32]	Present	Ref. [32]	Present
1	1.734	1.668	1.621	1.568
2	4.332	4.116	4.046	3.865
3	4.332	4.116	4.046	3.865
4	6.869	6.506	6.405	6.100
5	8.902	8.067	8.269	7.556

5.3. New Results for the Effect of The Agglomeration on FG-CNTRs Square Plates Free Vibrations Behavior

The free vibration behavior of a square plate, as shown in Fig. 1, was evaluated in the following subsections using the element Q9 with 16 x 16 elements (Table 4). In this section, various aspect ratio variations such as 5, 10, 20, 50, and 100 are taken for the purpose of analysis, along with a variety of boundary conditions. A complete parametric study is also done to find out more about the three-agglomeration stage. Different levels of agglomeration were tested on UD, FG-V, FG-X and FG-O type of carbon nanotube distribution.

Table 4. Convergence study for the dimensional frequency of an agglomerated CNT-reinforced plate with simply supported boundary conditions.

Mesh Size	UD	FG-V	FG-X	FG-O
8 x 8	15.823	13.822	18.800	12.157
10 x 10	15.819	13.817	18.796	12.153
12 x 12	15.817	13.815	18.795	12.151
14 x 14	15.817	13.814	18.794	12.150
16 x 16	15.816	13.814	18.794	12.150

The dimensionless frequencies used in this study were obtained using the following expressions:

$$\lambda = \omega \frac{a^2}{h}\sqrt{\frac{\rho_m}{E_m}} \tag{53}$$

After that, detailed parametric studies were carried out to investigate the effect of boundary conditions (SSSS, CCCC, SCSC, and SFSF), thickness ratio (a/h), agglomeration stage (ς, ξ), and CNT distribution pattern across the thickness direction on the free vibration behavior of an agglomerated CNT-reinforced FG plate. These studies were carried out in order to determine how these factors influence the behavior of the plate during free vibration. Tables (5)-(10) show the non-dimensional frequencies of the first six modes for three distinct types of agglomeration stages for the FG–CNT reinforced plate. The results are computed for a/b =1 and different aspect ratios as a/h = 5, 10, 20, 50, and 100. The minimum and maximum non-dimensional frequencies for the UD, FG-V, FG-X, and FG-O types of CNT distribution over the thickness were noted for all boundary conditions taken into consideration. As a result, the maximum and minimum stiffness are produced by the UD, FG-V, FG-X, and FG-O distributions, respectively. Additionally, it was discovered that the all-side-clamped plate produces the maximum frequency parameter whereas the SFSF produces the least frequency parameters.

This is because the stiffer agglomerated CNT-reinforced functionally graded plate results from the increased limitations at the boundary. Since the present study is based on the agglomeration effect of CNT, it can be seen through the result given in Table (5)-(10) for three stages of CNT agglomeration by varying the two-agglomeration parameter ς and ξ.

5.3.1. Free Vibration Analysis Without Agglomeration Effect

In this section agglomeration effect of CNT is not considered (ζ=ξ). The result presented in Table 5 is for without agglomeration effect of CNT with varying boundary conditions and aspect ratio. It can be seen that when compared to the other three distributions, the FG-X provides the best vibrational characteristics since its natural frequencies assume higher values. This behavior is attained because the CNTs are in higher concentrations distributed to higher stress regions. It could also be noted from Table 5 that the third mode was omitted since it is symmetrical with the second mode in case all edges are simply supported and clamped. As the aspect ratio increases the non-dimensional frequency also increases for all types of CNT distribution patterns considered in this study. But overall, one can observe that the FG-X pattern has higher stiffness as compared to other types of CNT distribution patterns. This means CNTs are present in the matrix without forming clusters. Further, the result is generated for the other two stages of the agglomeration effect as complete agglomeration and partial agglomeration stage by varying the ς and ξ parameters.

Table 5. The first six natural frequencies without the agglomeration effect for FG-CNT-reinforced plate with different boundary conditions ($V_{CNT}^{*}=0.075, \varsigma=\xi=0.5$).

CNT Distribution	a/h	Mode	SSSS	CCCC	SCSC	SFSF
UD CNT	5	1	14.548	22.370	18.233	14.297
		2	27.364	39.433	31.158	21.791
		3	27.364	39.433	35.611	27.364
		4	32.117	51.485	35.932	32.419
		5	32.117	51.485	37.690	33.499
		6	38.698	53.275	49.969	38.822
FG-V CNT		1	12.830	20.386	16.358	13.028
		2	27.488	36.346	31.242	19.694
		3	27.488	36.346	32.352	27.540
		4	28.688	49.285	32.628	30.641
		5	28.688	51.120	37.732	32.451
		6	38.648	51.120	45.652	34.745
FG-X CNT		1	16.550	23.590	19.890	15.272
		2	28.102	40.145	31.999	23.560
		3	28.102	40.145	37.318	28.102
		4	34.760	52.853	37.620	33.293
		5	34.760	52.853	38.695	34.794
		6	39.742	53.544	51.284	41.781
FG-O CNT		1	11.478	18.754	14.865	11.966
		2	26.203	34.176	30.005	18.394
		3	26.203	34.176	30.255	27.027
		4	27.027	46.712	30.775	28.537
		5	27.027	50.851	37.226	32.021
		6	38.223	50.851	42.760	32.028
UD CNT	10	1	15.816	27.091	21.016	17.315
		2	37.828	51.884	44.532	28.381
		3	37.828	51.884	44.809	42.565
		4	54.728	72.949	62.317	48.726
		5	54.728	86.138	65.393	54.728
		6	58.200	86.943	75.380	55.758
FG-V CNT		1	13.814	23.986	18.481	15.365
		2	33.216	46.327	39.440	25.748
		3	33.216	46.327	39.672	37.801
		4	51.330	65.450	58.184	43.216
		5	55.207	77.587	62.837	50.294
		6	55.207	78.288	70.228	55.036
FG-X CNT		1	18.794	30.923	24.457	19.793
		2	43.863	57.502	50.420	31.319
		3	43.863	57.502	50.778	47.960
		4	56.205	79.573	63.998	55.316
		5	56.205	92.781	72.770	56.205
		6	66.210	93.742	77.390	60.948

FG-O CNT	20	1	12.150	21.361	16.358	13.693
		2	29.489	41.763	35.294	23.604
		3	29.489	41.763	35.486	33.877
		4	45.922	59.477	52.479	39.169
		5	54.055	70.892	61.551	45.835
		6	54.055	71.454	63.636	54.055
UD CNT		1	16.211	29.024	22.026	18.691
		2	40.028	58.037	48.492	34.614
		3	40.028	58.037	48.721	44.660
		4	63.292	84.112	73.294	56.541
		5	78.496	101.299	89.696	65.314
		6	78.496	101.930	89.844	88.388
FG-V CNT		1	14.116	25.380	19.218	16.377
		2	34.911	50.913	42.414	31.021
		3	34.911	50.913	42.609	40.852
		4	55.288	73.979	64.242	50.490
		5	68.631	89.216	78.700	57.637
		6	68.631	89.746	78.824	77.590
FG-X CNT		1	19.560	34.529	26.394	22.184
		2	47.912	68.183	57.500	39.133
		3	47.912	68.183	57.797	55.223
		4	75.200	97.871	86.169	65.000
		5	92.843	117.163	104.928	75.659
		6	92.843	118.000	105.127	103.299
FG-O CNT		1	12.347	22.287	16.842	14.402
		2	30.623	44.903	37.306	27.883
		3	30.623	44.903	37.471	35.956
		4	48.631	65.491	56.689	45.557
		5	60.467	79.135	69.565	51.118
		6	60.467	79.579	69.669	68.604
UD CNT	50	1	16.337	29.706	22.365	19.315
		2	40.774	60.403	49.926	39.788
		3	40.774	60.403	50.133	48.212
		4	65.193	88.930	76.480	68.349
		5	81.291	107.793	94.114	69.924
		6	81.291	108.321	94.238	92.877
FG-V CNT		1	14.214	25.870	19.467	16.839
		2	35.490	52.640	43.482	35.009
		3	35.490	52.640	43.661	42.001
		4	56.786	77.592	66.673	60.849
		5	70.790	94.014	82.016	61.271
		6	70.790	94.466	82.123	80.946
FG-X CNT		1	19.804	35.912	27.075	23.295
		2	49.353	72.832	60.317	46.887
		3	49.353	72.832	60.573	58.202
		4	78.772	106.928	92.189	78.413
		5	98.169	129.526	113.384	83.830
		6	98.169	130.191	113.541	111.863
FG-O CNT		1	12.414	22.613	17.009	14.733
		2	31.014	46.055	38.021	30.883
		3	31.014	46.055	38.175	36.734
		4	49.672	67.978	58.365	53.505
		5	61.914	82.345	71.782	54.726
		6	61.914	82.733	71.874	70.849
UD CNT	100	1	16.382	29.902	22.470	19.511
		2	40.992	61.021	50.319	41.567
		3	40.992	61.021	50.516	48.618
		4	65.908	90.547	77.596	71.359
		5	81.961	109.303	95.147	76.095
		6	81.961	109.781	95.261	93.889
FG-V CNT		1	14.260	26.0514	19.568	17.001
		2	35.701	53.196	43.847	36.385
		3	35.701	53.196	44.016	42.357
		4	57.511	79.140	67.768	62.357
		5	71.400	95.307	82.924	67.227
		6	71.400	95.709	83.020	81.809

FG-X CNT	1	19.863	36.210	27.227	23.601
	2	49.665	73.818	60.917	49.761
	3	49.665	73.818	61.160	58.849
	4	79.704	109.246	93.729	86.005
	5	99.234	132.103	115.102	89.122
	6	99.234	132.705	115.245	113.585
FG-O CNT	1	12.459	22.779	17.104	14.868
	2	31.209	46.545	38.350	31.949
	3	31.209	46.545	38.494	37.040
	4	50.371	69.425	59.404	54.688
	5	62.436	83.418	72.546	59.514
	6	62.436	83.756	72.627	71.554

5.3.2. Free Vibration Analysis Under Complete Agglomeration Effect

The present section deals with the complete agglomeration effect assuming that all the CNTs are aggregated in the spherically shaped inclusion. Here, in this section, three different combinations of ζ and ξ are considered for the analysis of this particular agglomeration stage. As, we can see from Table 6–8 as parameter ξ increases from 0.25 to 0.75 corresponding to ζ=1, the stage where ξ is equal to 0.25 means all CNTs are presented in the matrix as circular clusters have less stiffness as compared to ξ= 0.75 stage. The stage ζ=1 and ξ= 0.25 represents the worst case of the agglomeration stage. Next, as the value of ξ reaches towards ζ the CNTs which are present in stage 1 in a cluster will try to free from cluster effect by uniform mixing with the surrounding matrix. Overall, from Table 6 to Table 8 it can easily be understood that case 3 where ζ=1 and ξ= 0.75 shows a higher value of nondimensional frequency as compared to the other two stages under the complete agglomeration effect.

According to the findings of the study, the elasticity of the material would be impacted more by the agglomeration of carbon nanotubes in proportion to the degree to which the values of the agglomeration parameters differed from one another. The same explanation can also be understood by glancing at the illustration that is labeled Fig. 9. The difference in the nondimensional frequency distributions is quite significant when contrasted with the frequency distributions of other cases of complete agglomeration. The difference between the two groups of findings is rather substantial when measured against the frequencies that were acquired in the section before this one without the agglomeration stage. The natural frequencies obtained for three different cases of complete agglomeration considering the UD, FG-V, FG-X, and FG-O are listed in Table 6 – 8. From this table, one can conclude that for all cases of complete agglomeration observed, the FG-O is the CNT distribution that has the worse dynamic behavior, when comparing it with the same states of agglomeration for the other CNT distributions.

When taken as a whole, it is possible to state that, for a stage that has been entirely agglomerated, the three CNT distributions that are being investigated will have lower natural frequencies if the distribution is more heterogeneous. It is possible to arrive at the conclusion that the FG-X distribution demonstrates superior vibrational behavior in addition to the level of agglomeration because CNTs are distributed in regions with higher bending stress; despite this, the differences in natural frequencies between the distributions become smaller as the value of ξ decreases.

Table 6. The first six non-dimensional natural frequencies for FG-CNT-reinforced plate with a full agglomeration effect with different boundary conditions $(V_{CNT}^{*}=0.075, \varsigma=1, \xi=0.25)$.

CNT Distribution	a/h	Mode	SSSS	CCCC	SCSC	SFSF
UD CNT	5	1	6.689	10.212	8.351	6.498
		2	12.263	17.935	13.973	9.906
		3	12.263	17.935	16.246	12.263
		4	14.706	23.532	16.394	14.554
		5	14.706	23.532	17.150	15.226
		6	17.343	24.193	22.750	17.733
FG-V CNT		1	6.535	10.021	8.178	6.372
		2	12.105	17.637	13.793	9.709
		3	12.105	17.637	15.946	12.105
		4	14.404	23.235	16.092	14.367
		5	14.404	23.235	16.933	14.955
		6	17.119	23.808	22.355	17.375

FG-X CNT		1	6.704	10.210	8.357	6.498
		2	12.225	17.909	13.930	9.907
		3	12.225	17.909	16.238	12.225
		4	14.715	23.461	16.386	14.510
		5	14.715	23.461	17.098	15.213
		6	17.289	24.147	22.724	17.737
FG-O CNT		1	6.527	10.025	8.1755	6.3744
		2	12.134	17.661	13.826	9.7129
		3	12.134	17.661	15.957	12.134
		4	14.402	23.291	16.103	14.402
		5	14.402	23.291	16.973	14.969
		6	17.161	23.848	22.380	17.38
UD CNT	10	1	7.298	12.458	9.681	7.942
		2	17.419	23.800	20.467	12.908
		3	17.419	23.800	20.596	19.541
		4	24.526	33.410	27.946	22.345
		5	24.526	39.409	30.007	24.526
		6	26.763	39.785	34.300	25.431
FG-V CNT		1	7.114	12.170	9.447	7.756
		2	17.003	23.286	20.001	12.631
		3	17.003	23.286	20.126	19.094
		4	24.211	32.718	27.587	21.824
		5	24.211	38.621	29.352	24.210
		6	26.145	38.986	33.866	24.887
FG-X CNT		1	7.3233	12.487	9.708	7.960
		2	17.469	23.832	20.507	12.919
		3	17.469	23.832	20.637	19.576
		4	24.451	33.437	27.860	22.386
		5	24.451	39.425	30.050	24.451
		6	26.819	39.803	34.196	25.449
FG-O CNT		1	7.098	12.153	9.430	7.7483
		2	16.974	23.269	19.977	12.637
		3	16.974	23.269	20.102	19.081
		4	24.269	32.708	27.653	21.817
		5	24.269	38.620	29.329	24.269
		6	26.112	38.983	33.946	24.903
UD CNT	20	1	7.489	13.393	10.170	8.612
		2	18.480	26.755	22.371	15.794
		3	18.480	26.755	22.477	21.515
		4	29.204	38.744	33.790	25.869
		5	36.208	46.641	41.337	30.011
		6	36.208	46.936	41.407	40.725
FG-V CNT		1	7.294	13.055	9.909	8.395
		2	18.008	26.096	21.810	15.440
		3	18.008	26.096	21.913	20.976
		4	28.468	37.809	32.956	25.269
		5	35.303	45.528	40.327	29.289
		6	35.303	45.813	40.394	39.729
FG-X CNT		1	7.518	13.439	10.207	8.641
		2	18.547	26.839	22.447	15.821
		3	18.547	26.839	22.554	21.587
		4	29.304	38.853	33.895	25.925
		5	36.327	46.765	41.460	30.090
		6	36.327	47.061	41.530	40.845
FG-O CNT		1	7.276	13.025	9.885	8.377
		2	17.964	26.043	21.761	15.427
		3	17.964	26.043	21.864	20.932
		4	28.404	37.740	32.889	25.242
		5	35.227	45.451	40.249	29.245
		6	35.227	45.735	40.316	39.656
UD CNT	50	1	7.549	13.724	10.333	8.917
		2	18.839	27.900	23.064	18.291
		3	18.839	27.900	23.160	22.268
		4	30.117	41.065	35.324	31.236
		5	37.554	49.777	43.469	32.256
		6	37.554	50.022	43.527	42.895

FG-V CNT		1	7.352	13.367	10.064	8.687
		2	18.348	27.178	22.465	17.840
		3	18.348	27.178	22.559	21.691
		4	29.334	40.009	34.411	30.517
		5	36.579	48.497	42.346	31.432
		6	36.579	48.735	42.402	41.787
FG-X CNT		1	7.579	13.778	10.374	8.952
		2	18.914	28.008	23.155	18.348
		3	18.914	28.008	23.251	22.355
		4	30.234	41.220	35.459	31.303
		5	37.700	49.964	43.636	32.374
		6	37.700	50.211	43.694	43.059
FG-O CNT		1	7.332	13.332	10.037	8.664
		2	18.299	27.108	22.407	17.804
		3	18.299	27.108	22.500	21.635
		4	29.258	39.909	34.323	30.478
		5	36.484	48.376	42.238	31.356
		6	36.484	48.613	42.294	41.680
UD CNT	100	1	7.570	13.814	10.382	9.011
		2	18.939	28.188	23.246	19.161
		3	18.939	28.188	23.337	22.459
		4	30.441	41.808	35.833	32.938
		5	37.866	50.488	43.954	34.927
		6	37.866	50.710	44.007	43.372
FG-V CNT		1	7.372	13.455	10.111	8.777
		2	18.445	27.456	22.641	18.673
		3	18.445	27.456	22.730	21.875
		4	29.652	40.730	34.907	32.090
		5	36.880	49.178	42.811	34.081
		6	36.880	49.394	42.863	42.245
FG-X CNT		1	7.600	13.869	10.423	9.047
		2	19.015	28.299	23.338	19.230
		3	19.015	28.299	23.430	22.548
		4	30.559	41.967	35.972	33.063
		5	38.015	50.685	44.126	35.028
		6	38.015	50.909	44.180	43.543
FG-O CNT		1	7.352	13.419	10.084	8.754
		2	18.396	27.384	22.581	18.629
		3	18.396	27.384	22.670	21.817
		4	29.574	40.627	34.818	32.009
		5	36.782	49.050	42.699	34.017
		6	36.782	49.266	42.750	42.134

Table 7. The first six non-dimensional natural frequencies for FG-CNT-reinforced plate with a full agglomeration effect with different boundary conditions ($V^{*}_{CNT}=0.075, \varsigma=1, \xi=0.5$).

CNT Distribution	a/h	Mode	SSSS	CCCC	SCSC	SFSF
UD CNT	5	1	8.417	12.883	10.522	8.209
		2	15.567	22.654	17.734	12.513
		3	15.567	22.654	20.499	15.567
		4	18.532	29.670	20.685	18.465
		5	18.532	29.670	21.656	19.237
		6	22.016	30.574	28.725	22.365
FG-V CNT		1	7.893	12.226	9.9318	7.782
		2	15.079	21.620	17.176	11.842
		3	17.493	21.620	19.464	15.083
		4	17.493	28.738	19.639	17.882
		5	17.493	28.738	20.985	18.303
		6	21.317	29.235	27.353	21.129
FG-X CNT		1	8.518	12.909	10.590	8.235
		2	15.427	22.589	17.574	12.564
		3	15.427	22.589	20.523	15.427
		4	18.640	29.407	20.709	18.299
		5	18.640	29.407	21.463	19.231
		6	21.817	30.436	28.687	22.471

FG-O CNT	10	1	7.756	12.108	9.802	7.702
		2	15.106	21.510	17.209	11.729
		3	15.106	21.510	19.298	15.106
		4	17.276	28.808	19.472	17.919
		5	17.276	28.808	21.024	18.169
		6	21.363	29.128	27.176	20.898
UD CNT		1	9.172	15.676	12.174	10.000
		2	21.910	29.973	25.758	16.295
		3	21.910	29.973	25.919	24.596
		4	31.135	42.098	35.468	28.129
		5	31.135	49.676	37.785	31.135
		6	33.675	50.146	43.313	32.072
FG-V CNT		1	8.554	14.700	11.385	9.380
		2	20.495	28.223	24.177	15.394
		3	20.495	28.233	24.326	23.106
		4	30.166	39.734	34.364	26.415
		5	30.166	46.973	35.552	30.159
		6	31.578	47.408	41.980	30.297
FG-X CNT		1	9.329	15.868	12.352	10.125
		2	22.221	30.229	26.048	16.411
		3	22.221	30.229	26.214	24.866
		4	30.854	42.371	35.148	28.453
		5	30.854	49.916	38.128	30.854
		6	34.077	50.398	42.927	32.292
FG-O CNT		1	8.370	14.438	11.162	9.217
		2	20.102	27.804	23.768	15.217
		3	20.102	27.804	23.911	22.735
		4	30.212	39.216	34.418	26.015
		5	30.212	46.423	35.015	29.943
		6	31.031	46.843	42.049	30.212
UD CNT	20	1	9.408	16.831	12.778	10.828
		2	23.221	33.636	28.117	19.925
		3	23.221	33.636	28.251	27.045
		4	36.703	48.722	42.479	32.601
		5	45.510	58.662	51.974	37.775
		6	45.510	59.030	52.060	51.210
FG-V CNT		1	8.758	15.697	11.905	10.104
		2	21.637	31.418	26.231	18.740
		3	21.637	31.418	26.354	25.239
		4	34.230	45.568	39.673	30.607
		5	42.466	54.904	48.569	35.355
		6	42.466	55.242	48.649	47.859
FG-X CNT		1	9.586	17.122	13.009	11.011
		2	23.638	34.167	28.592	20.128
		3	23.638	34.167	28.729	27.496
		4	37.331	49.433	43.152	32.992
		5	46.265	59.477	52.767	38.298
		6	46.265	59.858	52.857	51.985
FG-O CNT		1	8.5583	15.357	11.641	9.889
		2	21.158	30.774	25.672	18.447
		3	21.158	30.774	25.791	24.707
		4	33.496	44.675	38.859	30.105
		5	41.574	53.858	47.594	34.689
		6	41.574	54.184	47.671	46.906
UD CNT	50	1	9.483	17.240	12.981	11.205
		2	23.665	35.052	28.975	23.018
		3	23.665	35.052	29.095	27.977
		4	37.834	51.596	44.379	39.388
		5	47.177	62.541	54.612	40.542
		6	47.177	62.849	54.684	53.892
FG-V CNT		1	8.823	16.046	12.079	10.433
		2	22.023	32.635	26.970	21.505
		3	22.053	32.635	27.082	26.044
		4	35.218	48.059	41.323	36.974
		5	43.914	58.253	50.850	37.783
		6	43.914	58.538	50.918	50.182

FG-X CNT		1	9.667	17.570	13.231	11.415
		2	24.121	35.710	29.526	23.381
		3	24.121	35.710	29.649	28.506
		4	38.553	52.547	45.210	39.851
		5	48.072	63.692	55.633	41.271
		6	48.072	64.007	55.707	54.898
FG-O CNT		1	8.6184	15.678	11.800	10.196
		2	21.514	31.892	26.352	21.066
		3	21.514	31.892	26.461	25.449
		4	34.412	46.980	40.386	36.342
		5	42.910	56.945	49.697	36.953
		6	42.910	57.222	49.763	49.045
UD CNT	100	1	9.509	17.354	13.041	11.321
		2	23.791	35.412	29.203	24.089
		3	23.791	35.412	29.317	28.215
		4	38.244	52.530	45.021	41.390
		5	47.567	63.428	55.217	43.976
		6	47.567	63.707	55.284	54.487
FG-V CNT		1	8.848	16.151	12.136	10.538
		2	22.140	32.964	27.180	22.458
		3	22.140	32.964	27.286	26.260
		4	35.607	48.930	41.927	38.556
		5	44.271	59.049	51.398	41.136
		6	44.271	59.307	51.459	50.716
FG-X CNT		1	9.693	17.688	13.293	11.537
		2	24.250	36.087	29.763	24.516
		3	24.250	36.087	29.880	28.756
		4	38.969	53.508	45.867	42.157
		5	48.481	64.631	56.271	44.627
		6	48.481	64.917	56.339	55.528
FG-O CNT		1	8.642	15.779	11.856	10.296
		2	21.629	32.209	26.555	21.967
		3	21.629	32.209	26.659	25.656
		4	34.796	47.830	40.978	37.691
		5	43.252	57.702	50.219	40.329
		6	43.252	57.952	50.279	49.552

Table 8. The first six non-dimensional natural frequencies for FG-CNT-reinforced plate with a full agglomeration effect with different boundary conditions $(V_{CNT}^{*}=0.075, \varsigma=1, \xi=0.75)$.

CNT Distribution	a/h	Mode	SSSS	CCCC	SCSC	SFSF
UD CNT	5	1	10.760	16.503	13.467	10.531
		2	20.054	29.052	22.840	16.050
		3	20.054	29.052	26.265	20.054
		4	23.719	37.995	26.503	23.774
		5	23.719	37.995	27.770	24.675
		6	28.360	39.229	36.828	28.645
FG-V CNT		1	9.673	15.147	12.242	9.653
		2	19.247	26.905	21.912	14.660
		3	19.247	26.905	24.107	19.266
		4	21.546	36.392	24.319	22.698
		5	21.546	36.392	26.651	22.841
		6	27.179	36.440	33.956	26.046
FG-X CNT		1	11.180	16.697	13.789	10.689
		2	19.798	29.015	22.549	16.342
		3	19.798	29.015	26.517	19.798
		4	24.243	37.520	26.754	23.472
		5	24.243	37.520	27.422	24.815
		6	27.999	39.005	36.925	29.205
FG-O CNT		1	9.1787	14.626	11.729	9.311
		2	19.215	26.271	21.885	14.202
		3	19.215	26.271	23.348	19.215
		4	20.677	35.711	23.554	22.081
		5	20.677	36.432	26.624	22.781
		6	27.174	36.432	33.050	25.106

UD CNT	10	1	11.712	20.037	15.553	12.799
		2	27.993	38.341	32.930	20.918
		3	27.993	38.341	33.136	31.472
		4	40.108	53.877	45.680	36.017
		5	40.108	63.595	48.330	40.108
		6	43.046	64.194	55.541	41.144
FG-V CNT		1	10.442	18.030	13.931	11.521
		2	25.073	34.724	29.665	19.070
		3	25.073	34.724	29.843	28.384
		4	38.537	48.978	43.701	32.453
		5	38.537	57.984	43.888	37.451
		6	38.700	58.512	52.695	38.503
FG-X CNT		1	12.341	20.837	16.278	13.307
		2	29.267	39.477	34.153	21.430
		3	29.267	39.477	34.378	32.581
		4	39.597	55.166	45.099	37.331
		5	39.597	64.831	49.832	39.597
		6	44.726	65.472	54.844	42.087
FG-O CNT		1	9.8153	17.082	13.148	10.923
		2	23.690	33.127	28.170	18.347
		3	23.690	33.127	28.332	26.988
		4	36.721	46.926	41.676	30.968
		5	38.430	55.726	43.771	35.964
		6	38.430	56.204	50.384	38.430
UD CNT	20	1	12.009	21.492	16.314	13.834
		2	29.647	42.963	35.906	25.534
		3	29.647	42.963	36.076	34.545
		4	46.867	62.247	54.257	41.746
		5	58.119	74.955	66.391	48.300
		6	58.119	75.425	66.502	65.421
FG-V CNT		1	10.678	19.166	14.526	12.349
		2	26.398	38.409	32.035	23.110
		3	26.398	38.409	32.184	30.837
		4	41.789	55.761	48.491	37.679
		5	51.863	67.220	59.388	43.336
		6	51.863	67.628	59.484	58.533
FG-X CNT		1	12.715	22.655	17.235	14.566
		2	31.311	45.105	37.808	26.410
		3	31.311	45.105	37.992	36.350
		4	49.382	65.143	56.974	43.393
		5	61.151	78.295	69.607	50.450
		6	61.151	78.809	69.728	68.567
FG-O CNT		1	10.006	18.005	13.628	11.612
		2	24.775	36.174	30.118	22.015
		3	24.775	36.174	30.255	29.006
		4	39.280	52.629	45.673	35.883
		5	48.795	63.518	55.992	40.958
		6	48.795	63.890	56.080	55.199
UD CNT	50	1	12.104	22.007	16.569	14.305
		2	30.207	44.412	36.986	29.426
		3	30.207	44.412	37.139	35.714
		4	48.295	65.870	56.653	50.442
		5	60.221	79.842	69.715	51.774
		6	60.221	80.234	69.808	68.798
FG-V CNT		1	10.754	19.565	14.725	12.726
		2	26.847	39.800	32.885	26.330
		3	26.847	39.800	33.020	31.759
		4	42.942	58.634	50.401	45.515
		5	53.544	71.064	62.016	46.141
		6	53.544	71.409	62.098	61.204
FG-X CNT		1	12.833	23.313	17.560	15.141
		2	32.013	47.362	39.173	30.897
		3	32.013	47.362	39.337	37.816
		4	51.151	69.656	59.957	52.417
		5	63.774	84.422	73.774	54.687
		6	63.774	84.843	73.873	72.796

FG-O CNT	100	1	10.068	18.326	13.789	11.928
		2	25.142	37.300	30.808	24.806
		3	25.142	37.300	30.934	29.758
		4	40.235	54.990	47.246	43.126
		5	50.167	66.644	58.131	43.425
		6	50.167	66.964	58.207	57.372
UD CNT		1	12.137	22.152	16.647	14.452
		2	30.368	45.203	37.277	30.769
		3	30.368	45.203	37.423	36.016
		4	48.821	67.064	57.476	52.847
		5	60.718	80.968	70.485	56.245
		6	60.718	81.323	70.569	69.552
FG-V CNT		1	10.785	19.694	14.796	12.851
		2	26.994	40.202	33.144	27.436
		3	26.994	40.202	33.273	32.021
		4	43.437	59.721	51.161	47.061
		5	53.981	72.022	62.679	50.443
		6	53.981	72.332	62.753	61.844
FG-X CNT		1	12.868	23.476	17.646	15.311
		2	32.189	47.887	39.500	32.479
		3	32.189	47.887	39.656	38.164
		4	51.707	70.966	60.846	55.906
		5	64.344	85.750	74.672	58.911
		6	64.344	86.133	74.763	73.687
FG-O CNT		1	10.099	18.447	13.857	12.040
		2	25.282	37.670	31.050	25.767
		3	25.282	37.670	31.169	29.997
		4	40.718	56.027	47.978	44.150
		5	50.566	67.498	58.728	47.617
		6	50.566	67.783	58.796	57.940

5.3.3. Free Vibration Analysis Under Partial Agglomeration Effect

Similarly, we can conclude the partial agglomeration effect in which some CNTs are present in cluster form and some CNTs are present in the matrix. In this partial agglomeration stage, two types of agglomeration stages were considered for the study in which ζ and ξ will have two different values to create a partial agglomeration stage. In the first stage where ζ= 0.25 and ξ= 0.5 by assuming the maximum number of CNTs are present in the cluster form, some CNTs will present in the matrix, while in the second stage ζ= 0.75 and ξ= 0.5 is used to show that maximum number of CNTs are present in matrix and only little percentage of CNTs are forming clusters of CNT. Comparing both stages reveals that their behavior with respect to nondimensional frequency parameters is nearly identical. Although significant differences were found for the natural frequencies when comparing both cases of agglomeration under the partial agglomeration stage with the results obtained without the agglomeration stage discussed in section 5.3.1. Here, one can see the natural mode shapes do not suffer much difference from the agglomeration effect, for these two partially agglomerated states. In Table 12, the first six nondimensional frequencies for the UD, FG-V, FG-X, and FG-O distributions are presented. The table shows highest nondimensional frequencies appear for ζ= 0.25, and once again the lesser the volume of CNTs inside the agglomerated inclusions, the better the dynamic free vibration behavior obtained in the CNT-reinforced composite. Despite the agglomeration impact, the natural mode morphologies remained constant when compared to the findings obtained without the agglomeration stage for all forms of CNT dispersion.

Table 9. The first six non-dimensional natural frequencies for FG-CNT-reinforced plate with a partial agglomeration effect under different boundary conditions. ($V_{CNT}^{*}=0.075, \varsigma=0.25, \xi=0.5$).

CNT Distribution	a/h	Mode	SSSS	CCCC	SCSC	SFSF
UD CNT	5	1	14.018	21.561	17.572	13.782
		2	26.390	38.010	30.049	21.006
		3	26.390	38.010	34.323	26.390
		4	30.952	49.620	34.633	31.264
		5	30.952	49.620	36.330	32.291
		6	37.322	51.357	48.165	37.416

FG-V CNT	10	1	12.439	19.744	15.851	12.618
		2	26.542	35.188	30.167	19.077
		3	26.542	35.188	31.337	26.593
		4	27.803	47.710	31.604	29.673
		5	27.803	49.339	36.415	31.339
		6	37.322	49.339	44.213	33.665
FG-X CNT		1	15.946	22.757	19.177	14.734
		2	27.124	38.749	30.884	22.722
		3	27.124	38.749	36.004	27.124
		4	33.521	50.973	36.297	32.132
		5	33.521	50.973	37.325	33.578
		6	38.359	51.693	49.497	40.299
FG-O CNT		1	11.131	18.173	14.410	11.595
		2	25.400	33.100	29.073	17.818
		3	25.400	33.100	29.315	26.090
		4	26.090	45.232	29.708	27.646
		5	26.090	49.052	35.915	30.908
		6	36.897	49.052	41.421	31.040
UD CNT	10	1	15.238	26.104	20.249	16.692
		2	36.448	49.998	42.911	27.378
		3	36.448	49.998	43.177	41.033
		4	52.781	70.301	60.099	46.988
		5	52.781	83.015	63.016	52.781
		6	56.080	83.790	72.661	53.789
FG-V CNT		1	13.397	23.252	17.919	14.895
		2	32.208	44.898	38.233	24.942
		3	32.208	44.898	38.457	36.641
		4	49.765	63.420	56.395	41.889
		5	53.302	75.172	60.668	48.729
		6	53.302	75.852	68.062	53.143
FG-X CNT		1	18.093	29.792	23.555	19.072
		2	42.247	55.427	48.582	30.197
		3	42.247	55.427	48.927	46.220
		4	54.249	76.722	61.769	53.300
		5	54.249	89.475	70.140	54.249
		6	63.793	90.400	74.651	58.776
FG-O CNT		1	11.786	20.715	15.866	13.278
		2	28.601	40.490	34.225	22.870
		3	28.601	40.490	34.411	32.850
		4	44.534	57.655	50.882	37.970
		5	52.181	68.712	59.416	44.425
		6	52.181	69.259	61.693	52.181
UD CNT	20	1	15.619	27.963	21.221	18.010
		2	38.565	55.919	46.721	33.367
		3	38.565	55.919	46.941	44.960
		4	60.979	81.043	70.618	54.502
		5	75.629	97.605	86.422	62.948
		6	75.629	98.213	86.565	85.169
FG-V CNT		1	13.691	24.612	18.638	15.881
		2	33.858	49.369	41.132	30.062
		3	33.858	49.369	41.320	39.615
		4	53.618	71.729	62.295	48.932
		5	66.556	86.499	76.312	55.880
		6	66.556	87.015	76.433	75.235
FG-X CNT		1	18.826	33.241	25.406	21.359
		2	46.120	65.655	55.359	37.719
		3	46.120	65.655	55.643	53.169
		4	72.396	94.258	82.973	62.616
		5	89.390	112.851	101.046	72.884
		6	89.390	113.655	101.237	99.481
FG-O CNT		1	11.978	21.620	16.339	13.971
		2	29.708	43.555	36.189	27.030
		3	29.708	43.555	36.349	34.878
		4	47.176	63.520	54.988	44.156
		5	58.655	76.752	67.476	49.577
		6	58.655	77.183	67.577	66.543

UD CNT	50	1	15.739	28.620	21.547	18.609
		2	39.282	58.194	48.100	38.340
		3	39.282	58.194	48.300	46.449
		4	62.809	85.679	73.684	65.875
		5	78.318	103.852	90.672	67.371
		6	78.318	104.361	90.792	89.482
FG-V CNT		1	13.787	25.091	18.881	16.331
		2	34.421	51.054	42.173	33.945
		3	34.421	51.054	42.346	40.736
		4	55.076	75.251	64.663	58.993
		5	68.658	91.178	79.545	59.402
		6	68.658	91.617	79.648	78.506
FG-X CNT		1	19.058	34.561	26.056	22.421
		2	47.496	70.096	58.050	45.153
		3	47.496	70.096	58.296	56.015
		4	75.810	102.917	88.727	75.553
		5	94.479	124.669	109.127	80.693
		6	94.479	125.309	109.278	107.664
FG-O CNT		1	12.044	21.938	16.502	14.292
		2	30.088	44.679	36.886	29.954
		3	30.088	44.679	37.036	35.637
		4	48.188	65.945	56.621	51.902
		5	60.066	79.884	69.638	53.056
		6	60.066	80.261	69.727	68.733
UD CNT	100	1	15.783	28.808	21.648	18.797
		2	39.493	58.789	48.479	40.049
		3	39.493	58.789	48.668	46.840
		4	63.498	87.237	74.760	68.751
		5	78.963	105.306	91.668	73.328
		6	78.963	105.767	91.778	90.455
FG-V CNT		1	13.831	25.266	18.979	16.489
		2	34.626	51.592	42.526	35.284
		3	34.626	51.592	42.689	41.081
		4	55.775	76.747	65.720	60.472
		5	69.248	92.433	80.425	65.177
		6	69.248	92.823	80.518	79.344
FG-X CNT		1	19.115	34.847	26.202	22.713
		2	47.795	71.041	58.624	47.902
		3	47.795	71.041	58.858	56.634
		4	76.706	105.140	90.205	82.777
		5	95.499	127.135	110.772	85.839
		6	95.499	127.714	110.909	109.312
FG-O CNT		1	12.087	22.098	16.593	14.423
		2	30.276	45.153	37.203	30.990
		3	30.276	45.153	37.343	35.933
		4	48.862	67.341	57.622	53.047
		5	60.571	80.922	70.377	57.7156
		6	60.571	81.251	70.456	69.416

Table 10. The first six non-dimensional natural frequencies for FG-CNT-reinforced plate with a partial agglomeration effect under different boundary conditions $(V_{CNT}^{*}=0.075, \varsigma=0.75,\ \xi=0.5)$.

CNT Distribution	a/h	Mode	SSSS	CCCC	SCSC	SFSF
UD CNT	5	1	13.632	20.962	17.085	13.397
		2	25.640	36.950	29.196	20.419
		3	25.640	36.950	33.369	25.640
		4	30.095	48.243	33.670	30.377
		5	30.095	48.243	35.317	31.389
		6	36.261	49.921	46.822	36.377
FG-V CNT		1	12.134	19.231	15.450	12.287
		2	25.705	34.259	29.220	18.581
		3	25.705	34.259	30.530	25.754
		4	27.109	46.445	30.790	28.895
		5	27.109	47.854	35.295	30.366
		6	36.158	47.854	43.067	32.810

FG-X CNT		1	15.422	22.081	18.581	14.282
		2	26.270	37.650	29.913	22.011
		3	26.270	37.650	34.945	26.270
		4	32.496	49.404	35.231	31.123
		5	32.496	49.404	36.171	32.595
		6	37.152	50.255	48.087	39.072
FG-O CNT		1	10.891	17.752	14.087	11.323
		2	24.831	32.301	28.395	17.386
		3	24.831	32.301	28.632	25.299
		4	25.299	44.122	28.808	26.990
		5	25.299	47.599	34.846	29.974
		6	35.779	47.599	40.435	30.327
UD CNT	10	1	14.821	25.385	19.693	16.231
		2	35.447	48.617	41.729	26.613
		3	35.447	48.617	41.988	39.901
		4	51.281	68.356	58.392	45.688
		5	51.281	80.715	61.276	51.281
		6	54.536	81.469	70.634	52.291
FG-V CNT		1	13.072	22.675	17.480	14.522
		2	31.421	43.770	37.286	24.286
		3	31.421	43.770	37.506	35.728
		4	48.544	61.817	54.989	40.841
		5	51.607	73.261	58.740	47.475
		6	51.607	73.925	66.358	51.463
FG-X CNT		1	17.462	28.807	22.755	18.437
		2	40.821	53.667	46.995	29.221
		3	40.821	53.667	47.327	44.718
		4	52.541	74.337	59.827	51.538
		5	52.541	86.740	67.900	52.541
		6	61.697	87.636	72.342	56.923
FG-O CNT		1	11.539	20.269	15.529	12.989
		2	27.993	39.597	33.483	22.328
		3	27.993	39.597	33.666	32.133
		4	43.573	56.362	49.763	37.115
		5	50.599	67.156	57.616	43.409
		6	50.599	67.693	60.324	50.599
UD CNT	20	1	15.191	27.196	20.635	17.515
		2	37.508	54.384	45.439	32.440
		3	37.508	54.384	45.653	43.726
		4	59.307	78.816	68.680	52.991
		5	73.555	94.922	84.049	61.212
		6	73.555	95.513	84.188	82.829
FG-V CNT		1	13.360	24.014	18.187	15.493
		2	33.039	48.163	40.132	29.291
		3	33.039	48.163	40.316	38.650
		4	52.318	69.970	60.776	47.681
		5	64.940	84.374	74.449	54.497
		6	64.940	84.878	74.567	73.396
FG-X CNT		1	18.154	32.079	24.508	20.613
		2	44.493	63.398	53.432	36.467
		3	44.493	63.398	53.705	51.322
		4	69.869	91.060	80.118	60.489
		5	86.290	109.055	97.594	70.417
		6	86.290	109.828	97.777	96.087
FG-O CNT		1	11.730	21.167	15.998	13.676
		2	29.088	42.636	35.429	26.421
		3	29.088	42.636	35.587	34.145
		4	46.187	62.170	53.827	43.147
		5	57.423	75.115	66.048	48.512
		6	57.423	75.538	66.147	65.133
UD CNT	50	1	15.309	27.836	20.957	18.099
		2	38.207	56.601	46.783	37.284
		3	38.207	56.601	46.977	45.177
		4	61.089	83.332	71.666	64.047
		5	76.174	101.007	88.189	65.523
		6	76.174	101.502	88.306	87.031

FG-V CNT	100	1	13.454	24.484	18.425	15.936
		2	33.590	49.818	41.154	33.107
		3	33.590	49.818	41.323	39.751
		4	53.744	73.426	63.097	57.518
		5	67.000	88.970	77.621	57.926
		6	67.000	89.398	77.722	76.607
FG-X CNT		1	18.374	33.325	25.123	21.621
		2	45.794	67.599	55.975	43.585
		3	45.794	67.599	56.213	54.016
		4	73.100	99.263	85.566	72.993
		5	91.105	120.248	105.243	77.835
		6	91.105	120.864	105.389	103.834
FG-O CNT		1	11.794	21.483	16.160	13.995
		2	29.465	43.750	36.120	29.314
		3	29.465	43.750	36.267	34.897
		4	47.186	64.568	55.441	50.813
		5	58.819	78.220	68.190	51.869
		6	58.819	78.589	68.277	67.304
UD CNT		1	15.351	28.019	21.055	18.282
		2	38.411	57.180	47.151	38.950
		3	38.411	57.180	47.336	45.557
		4	61.759	84.847	72.712	66.867
		5	76.801	102.422	89.158	71.304
		6	76.801	102.871	89.265	87.978
FG-V CNT		1	13.497	24.654	18.520	16.090
		2	33.788	50.341	41.496	34.421
		3	33.788	50.341	41.655	40.087
		4	54.419	74.875	64.120	58.998
		5	67.573	90.191	78.476	63.552
		6	67.573	90.573	78.568	77.423
FG-X CNT		1	18.429	33.597	25.261	21.900
		2	46.080	68.496	56.522	46.206
		3	46.080	68.496	56.747	54.604
		4	73.957	101.381	86.976	79.822
		5	92.074	122.586	106.803	82.871
		6	92.074	123.144	106.936	105.396
FG-O CNT		1	11.836	21.638	16.248	14.123
		2	29.647	44.211	36.428	30.336
		3	29.647	44.211	36.565	35.185
		4	47.837	65.920	56.410	51.930
		5	59.310	79.232	68.909	56.466
		6	59.310	79.555	68.987	67.970

The influence that the side-to-thickness ratio has on the nondimensional fundamental frequency of FG-CNT reinforced plate is illustrated in Fig. (10)-(15). For the different boundary conditions of SSSS, CCCC, SCSC, and SFSF, the results are calculated for V_{CNT}^{*} =0.075. Here, it can be seen that the a/h ratio increases with increasing dimensionless frequency parameters, and it becomes insensitive after a/h = 50 for all applied boundary conditions.

Overall, from the three stages of the agglomeration effect, without agglomeration stage led to give higher non-dimensional frequency as compared to the other two stages because nonuniform CNT distribution in the matrix affects the overall material properties of the nanocomposite. The effect if not considered will propagate the erroneous overall result.

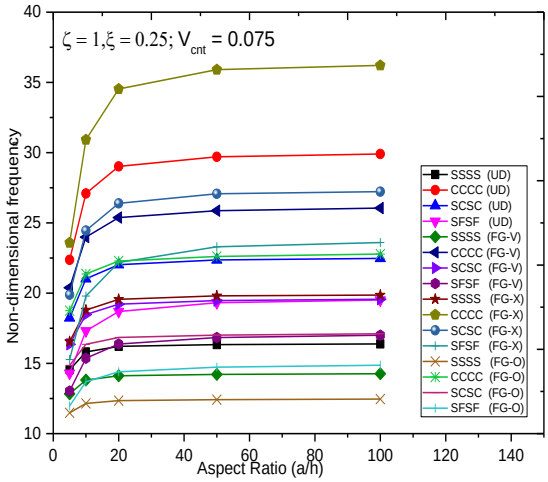

Fig. 10. Variation of dimensionless frequency vs. a/h ratio for different types of CNT-reinforced plate with various boundary conditions, including without agglomeration effect

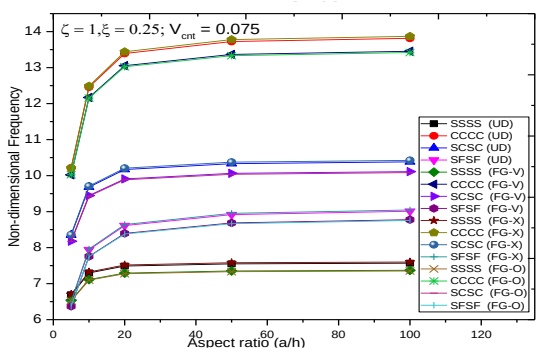

Fig. 11. Variation of dimensionless frequency vs. a/h ratio for different types of CNT-reinforced plate with various boundary conditions for complete agglomeration effect (Case-1).

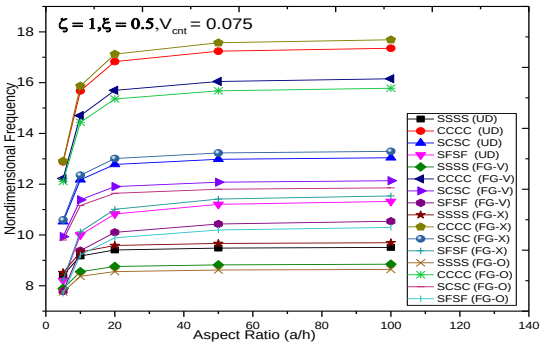

Fig. 12. Variation of dimensionless frequency vs. a/h ratio for different types of CNT-reinforced plate with various boundary conditions for complete agglomeration effect (Case-2).

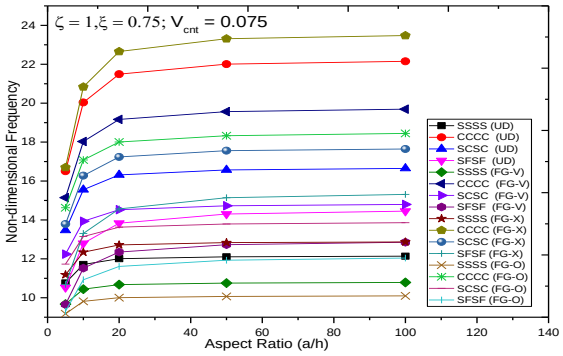

Fig. 13. Variation of dimensionless frequency vs. a/h ratio for different types of CNT-reinforced plate with various boundary conditions for complete agglomeration effect (Case-3)

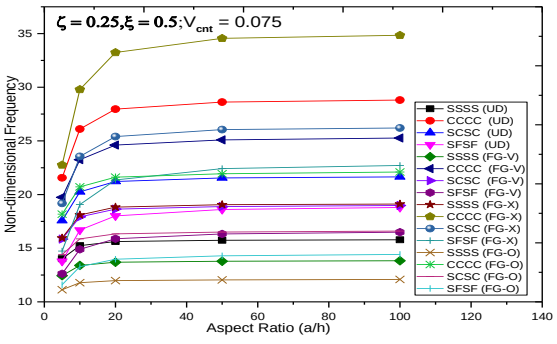

Fig. 14. Variation of dimensionless frequency vs. a/h ratio for different types of CNT-reinforced plate with various boundary conditions for partial agglomeration effect (Case-1)

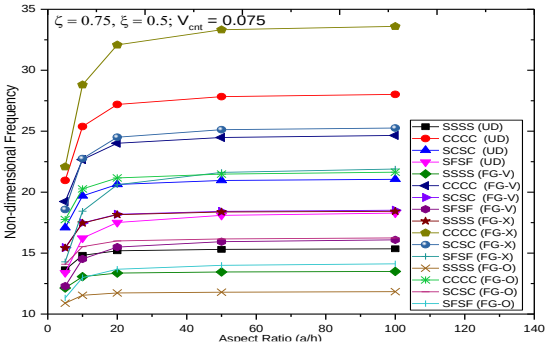

Fig. 15. Variation of dimensionless frequency vs. a/h ratio for different types of CNT-reinforced plate with various boundary conditions for partial agglomeration effect (Case-2)

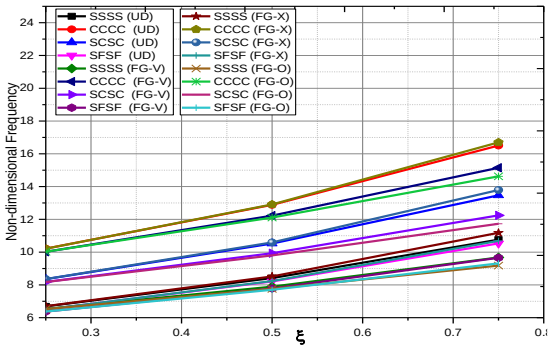

Fig. 16. Variation of dimensionless frequency vs. agglomeration parameter ξ for different types of CNT reinforced plate with different boundary conditions for complete agglomeration effect for a/h =5 (Case-1)

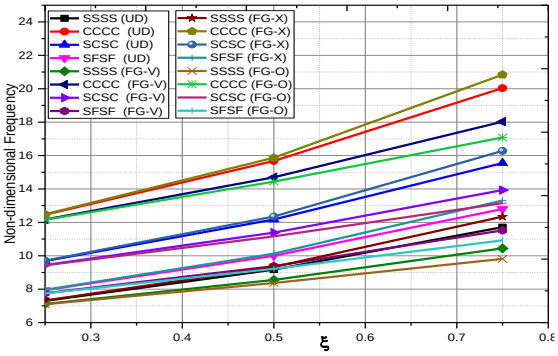

Fig. 17. Variation of dimensionless frequency vs. agglomeration parameter ξ for different types of CNT reinforced plate with different boundary conditions for complete agglomeration effect for a/h =10 (Case-2)

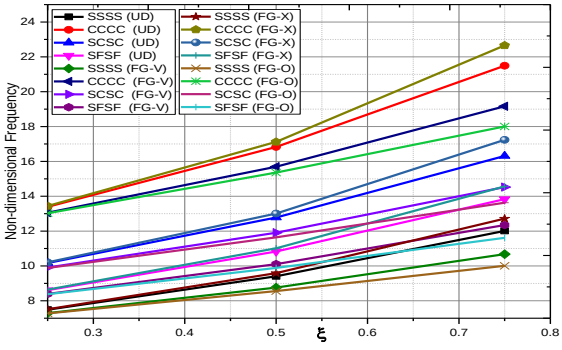

Fig. 18. Variation of dimensionless frequency vs. agglomeration parameter ξ for different types of CNT-reinforced plate with different boundary conditions for complete agglomeration effect for a/h =20 (Case-3)

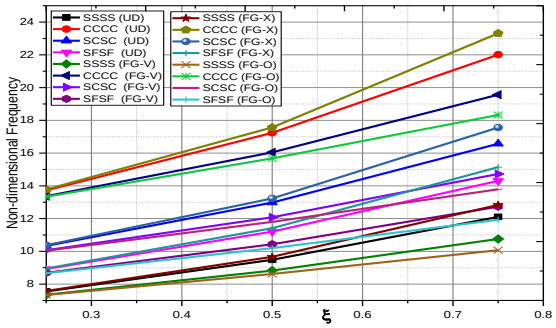

Fig. 19. Variation of dimensionless frequency vs. agglomeration parameter ξ for different types of CNT reinforced plate with different boundary conditions for complete agglomeration effect for a/h =50 (Case-3).

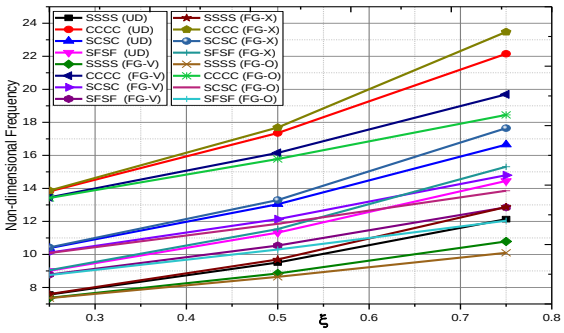

Fig. 20. Variation of dimensionless frequency vs. agglomeration parameter ξ for different types of CNT reinforced plate with different boundary conditions for complete agglomeration effect for a/h =100 (Case-5)

6. Conclusions

In the current work, an investigation into the free vibration behavior of CNT-reinforced functionally graded plates, including the effect of agglomeration, was carried out using a C0 FE model that was developed using Reddy's HSDT. It is presumed that the CNT distribution will be uniform or functionally graded all the way through the thickness of the plate. The Eshelby-Mori-Tanaka approach, which is based on a two-parameter model ζ and ξ, is utilized in order to compute the properties of an agglomerated CNT-reinforced composite plate at any point. By adjusting these two parameters, it was possible to capture all three stages of the agglomeration effect. Several parametric studies were conducted to determine the effect of reinforcing phase features such as agglomeration and volume fraction distribution along the thickness. These studies examine how these factors affect the dynamic behavior of these structures.

The most important contribution of this work was the introduction of the carbon nanotube agglomeration model into the constitutive rules that define mechanical behavior. In addition, Reddy's well-known HSDT model is utilized in order to perform an analysis of the free vibrations of plates with varying parameters such as aspect ratio, CNT distribution across the thickness, and three distinct stages of agglomeration. The overall concise outcomes of the present study are as follows:

- The FG-X type distribution of carbon nanotubes along the thickness direction provided higher natural frequencies when compared to the other three distributions that were considered for the same state of agglomeration. This was the case regardless of whether or not there was any agglomeration present, in any of the three different cases of complete agglomeration, or either of the two states of partial agglomeration. This is due to a larger concentration of carbon nanotubes in locations that experience significant levels of bending stress.
- According to the findings of the study, having a lower value for the parameter ξ causes the free vibration behavior of these structures to worsen, which in turn results in lower natural frequencies for all of the other three CNT distribution patterns.
- Similarly, the partial agglomeration stage concludes that the higher the agglomeration parameter ζ, the lower the natural frequencies for the carbon nanotube distributions considered.
- There is an increase in dimensionless frequency with an increased aspect ratio.
- Greater boundary restrictions produce higher values for the dimensionless frequency parameters.
- Among the three stages of the agglomeration effect of CNTs, the without agglomeration stage led to higher non-dimensional frequency parameters as compared to the complete agglomeration stage and partial agglomeration stage.

Nomenclature

CNT	Carbon nanotube
FG	Functionally Graded Materials
h	Thickness
UD	Uniformly Distributed
V_{cnt}^{*}	Carbon nanotube volume fraction
SSSS	All four edges simply supported
CCCC	All four edges clamped
SCSC	Two adjacent edges simply supported and the remaining two adjacent edges clamped
SFSF	Two adjacent edges simply supported and the remaining two adjacent edges Free
FG-V	V-Type CNT distribution pattern along the thickness direction
FG-X	X-Type CNT distribution pattern along the thickness direction
FG-O	O-Type CNT distribution pattern along the thickness direction
ζ, ξ	Agglomeration parameter
N_i	Shape function

Acknowledgments

The authors would like to acknowledge Madan Mohan Malaviya University of Technology, Gorakhpur U.P-273010 India, for the financial support of this work.

Conflicts of Interest

The corresponding author declares that there are no competing interests on behalf of the other authors.

References

[1] Iijima, S., 1991. Helical microtubules of graphitic carbon. nature, 354(6348), pp.56-58.

[2] Iijima, S. and Ichihashi, T., 1993. Single-shell carbon nanotubes of 1-nm diameter. nature, 363(6430), pp.603-605.

[3] Liew, K.M., Lei, Z.X. and Zhang, L.W., 2015. Mechanical analysis of functionally graded carbon nanotube reinforced composites: a review. Composite Structures, 120, pp.90-97.

[4] Aragh, B.S., Barati, A.N. and Hedayati, H., 2012. Eshelby–Mori–Tanaka approach for vibrational behavior of continuously graded carbon nanotube-reinforced cylindrical panels. Composites Part B: Engineering, 43(4), pp.1943-1954.

[5] Mareishi, S., Kalhori, H., Rafiee, M. and Hosseini, S.M., 2015. Nonlinear forced vibration response of smart two-phase nano-composite beams to external harmonic excitations. Curved and Layered Structures, 2(1).

[6] Alibeigloo, A. and Liew, K.M., 2013. Thermoelastic analysis of functionally graded carbon nanotube-reinforced composite plate using theory of elasticity. Composite Structures, 106, pp.873-881.

[7] Alibeigloo, A., 2014. Free vibration analysis of functionally graded carbon nanotube-reinforced composite cylindrical panel embedded in piezoelectric layers by using theory of elasticity. European Journal of Mechanics-A/Solids, 44, pp.104-115.

[8] Zhang, L.W., Lei, Z.X. and Liew, K.M., 2015. Vibration characteristic of moderately thick functionally graded carbon nanotube reinforced composite skew plates. Composite Structures, 122, pp.172-183.

[9] Zhang, L.W., Lei, Z.X. and Liew, K.M., 2015. Computation of vibration solution for functionally graded carbon nanotube-reinforced composite thick plates resting on elastic foundations using the element-free IMLS-Ritz method. Applied Mathematics and Computation, 256, pp.488-504..

[10] Shi, D.L., Feng, X.Q., Huang, Y.Y., Hwang, K.C. and Gao, H., 2004. The effect of nanotube waviness and agglomeration on the elastic property of carbon nanotube-reinforced composites. J. Eng. Mater. Technol., 126(3), pp.250-257.

[11] Mori, T. and Tanaka, K., 1973. Average stress in matrix and average elastic energy of materials with misfitting inclusions. Acta metallurgica, 21(5), pp.571-574.

[12] Hedayati, H. and Aragh, B.S., 2012. Influence of graded agglomerated CNTs on vibration of CNT-reinforced annular sectorial plates resting on Pasternak foundation. Applied Mathematics and Computation, 218(17), pp.8715-8735.

[13] Aragh, B.S., Farahani, E.B. and Barati, A.N., 2013. Natural frequency analysis of continuously graded carbon nanotube-reinforced cylindrical shells based on third-order shear deformation theory. Mathematics and Mechanics of Solids, 18(3), pp.264-284.

[14] Formica, G., Lacarbonara, W. and Alessi, R., 2010. Vibrations of carbon nanotube-reinforced composites. Journal of sound and vibration, 329(10), pp.1875-1889.

[15] Hosseini-Hashemi, S., Taher, H.R.D., Akhavan, H. and Omidi, M., 2010. Free vibration of functionally graded rectangular plates using first-order shear deformation plate theory. Applied Mathematical Modelling, 34(5), pp.1276-1291.

[16] Ramu, I. and Mohanty, S.C., 2012. Study on free vibration analysis of rectangular plate structures using finite element method. Procedia engineering, 38, pp.2758-2766.

[17] Thai, H.T. and Kim, S.E., 2013. A simple higher-order shear deformation theory for bending and free vibration analysis of functionally graded plates. Composite Structures, 96, pp.165-173.

[18] Tornabene, F., Fantuzzi, N., Bacciocchi, M. and Viola, E., 2016. Effect of agglomeration on the natural frequencies of functionally graded carbon nanotube-reinforced laminated composite doubly-curved shells. Composites Part B: Engineering, 89, pp.187-218.

[19] Kiani, Y., 2016. Free vibration of functionally graded carbon nanotube reinforced composite plates integrated with piezoelectric layers. Computers & Mathematics with Applications, 72(9), pp.2433-2449.

[20] Van Long, N., Quoc, T.H. and Tu, T.M., 2016. Bending and free vibration analysis of functionally graded plates using new eight-unknown shear deformation theory by finite-element method. International journal

of advanced structural engineering, 8(4), pp.391-399.
[21] Moghadam, H.Z., Faghidian, S.A. and Jamal-Omidi, M., 2018. Agglomeration effects of carbon nanotube on residual stresses in polymer nano composite using experimental and analytical method. Materials Research Express, 6(3), p.035009.
[22] Daghigh, H. and Daghigh, V., 2019. Free vibration of size and temperature-dependent carbon nanotube (CNT)-reinforced composite nanoplates with CNT agglomeration. Polymer Composites, 40(S2), pp.E1479-E1494.
[23] Tavakoli Maleki, A., Pourseifi, M. and Zakeri, M., 2022. Effect of agglomeration of the nanotubes on the vibration frequency of the multi-scale hybrid nanocomposite conical shells: a GDQ-based study. Waves in Random and Complex Media, 32(1), pp.359-380.
[24] Eshelby, J.D., 1957. The determination of the elastic field of an ellipsoidal inclusion, and related problems. Proceedings of the royal society of London. Series A. Mathematical and physical sciences, 241(1226), pp.376-396.
[25] Benveniste, Y., 1987. A new approach to the application of Mori-Tanaka's theory in composite materials. Mechanics of materials, 6(2), pp.147-157.
[26] Shokrieh, M.M. and Rafiee, R., 2010. On the tensile behavior of an embedded carbon nanotube in polymer matrix with non-bonded interphase region. Composite Structures, 92(3), pp.647-652.
[27] Yas, M.H. and Heshmati, M., 2012. Dynamic analysis of functionally graded nanocomposite beams reinforced by randomly oriented carbon nanotube under the action of moving load. Applied Mathematical Modelling, 36(4), pp.1371-1394.
[28] Kamarian, S., Shakeri, M., Yas, M.H., Bodaghi, M. and Pourasghar, A., 2015. Free vibration analysis of functionally graded nanocomposite sandwich beams resting on Pasternak foundation by considering the agglomeration effect of CNTs. Journal of Sandwich Structures & Materials, 17(6), pp.632-665.
[29] Taj, M.G., Chakrabarti, A. and Sheikh, A.H., 2013. Analysis of functionally graded plates using higher order shear deformation theory. Applied Mathematical Modelling, 37(18-19), pp.8484-8494.
[30] Stephan, C., Nguyen, T.P., De La Chapelle, M.L., Lefrant, S., Journet, C. and Bernier, P., 2000. Characterization of singlewalled carbon nanotubes-PMMA composites. Synthetic Metals, 108(2), pp.139-149.
[31] Shen, L. and Li, J., 2004. Transversely isotropic elastic properties of single-walled carbon nanotubes. Physical Review B, 69(4), p.045414.
[32] Talha, M. and Singh, B., 2010. Static response and free vibration analysis of FGM plates using higher order shear deformation theory. Applied Mathematical Modelling, 34(12), pp.3991-4011.
[33] Odegard, G.M., Gates, T.S., Wise, K.E., Park, C. and Siochi, E.J., 2003. Constitutive modeling of nanotube–reinforced polymer composites. Composites science and technology, 63(11), pp.1671-1687.
[34] Zhang, L.W., Zhang, Y., Zou, G.L. and Liew, K.M., 2016. Free vibration analysis of triangular CNT-reinforced composite plates subjected to in-plane stresses using FSDT element-free method. Composite structures, 149, pp.247-260.
[35] Zhang, L.W., 2017. On the study of the effect of in-plane forces on the frequency parameters of CNT-reinforced composite skew plates. Composite Structures, 160, pp.824-837.
[36] Zhang, L.W. and Selim, B.A., 2017. Vibration analysis of CNT-reinforced thick laminated composite plates based on Reddy's higher-order shear deformation theory. Composite Structures, 160, pp.689-705.
[37] Mehar, K. and Kumar Panda, S., 2018. Thermal free vibration behavior of FG-CNT reinforced sandwich curved panel using finite element method. Polymer Composites, 39(8), pp.2751-2764.
[38] Mehar, K., Panda, S.K. and Mahapatra, T.R., 2017. Theoretical and experimental investigation of vibration characteristic of carbon nanotube reinforced polymer composite structure. International Journal of Mechanical Sciences, 133, pp.319-329.
[39] Mehar, K., Panda, S.K. and Patle, B.K., 2018. Stress, deflection, and frequency analysis of CNT reinforced graded sandwich plate under uniform and linear thermal environment: A finite element approach. Polymer Composites, 39(10), pp.3792-3809.
[40] Mehar, K., Panda, S.K. and Patle, B.K., 2017. Thermoelastic vibration and flexural behavior of FG-CNT reinforced composite curved panel. International Journal of Applied Mechanics, 9(04), p.1750046.
[41] Liew, K.M., Pan, Z. and Zhang, L.W., 2020. The recent progress of functionally graded CNT reinforced composites and structures. Science China Physics, Mechanics & Astronomy, 63(3), pp.1-17.